JOURNAL OF PLANKTON RESEARCH | VOLUME 23 | NUMBER 2 | PAGES 117–141 | 2001

Universal multifractals and ocean patchiness: phytoplankton, physical fields and coastal heterogeneity

S. LOVEJOY[1], W. J. S. CURRIE[3], Y. TESSIER[1,6], M. R. CLAEREBOUDT[2,5], E. BOURGET[2], J. C. ROFF[3] AND D. SCHERTZER[4]
[1]PHYSICS DEPARTMENT AND GIROQ (GROUPE INTERUNIVERSITAIRE DE RECHERCHES OCÉANOGRAPHIQUES DU QUÉBEC), MCGILL UNIVERSITY, 3600 UNIVERSITY STREET, MONTRÉAL, QUÉBEC, H3A 2T8, [2]DÉPARTEMENT DE BIOLOGIE ET CIROQ, PAVILLON VACHON, UNIVERSITÉ LAVAL, QUÉBEC, QUÉBEC, G1K 7P4, [3]DEPARTMENT OF ZOOLOGY, COLLEGE OF BIOLOGICAL SCIENCE, UNIVERSITY OF GUELPH, GUELPH, ONTARIO, N1G 2W1, CANADA, [4]LABORATOIRE DE MODÉLISATION EN MÉCANIQUE, BP 162, U. PIERRE ET MARIE-CURIE, 4 PL. JUSSIEU, PARIS, 75005, FRANCE, [5]SULTAN QABOOS UNIVERSITY, FACULTY OF AGRICULTURE, DEPARTMENT OF FISHERIES, PO BOX 34, AL-KHOD 123, SULTANATE OF OMAN AND [6]RESEARCH AND DEVELOPMENT, LOCKHEED MARTIN ELECTRONIC SYSTEMS CANADA, 6111 ROYALMOUNT AVENUE, MONTREAL, QUEBEC, H4P 1K6, CANADA

We argue that a wide-range scaling approach is demanded by standard Stommel diagrams and that it can unify the treatment of phytoplankton variability over wide ranges of scales. By investigating the effects of coastal heterogeneity on the variability of in situ salinity (S), oxygen (ρ_O), temperature (T), optical transmissivity (t) and phytoplankton proxy data (fluorescence; ρ_p) over the range ~0.4–1600 m, we statistically characterize the heterogeneity of these variables, determining both the range and types of scaling, as well as their scale-by-scale interrelationships. By comparing bays with systematically varying large-scale heterogeneity, we were able to investigate the influence of the latter on the variability, systematically determining the three universal multifractal parameters as well as the exponent characterizing extreme self-organized critical behaviour. We found that, consistent with turbulent dominated dynamics, T, ρ_O, S and t were scaling over essentially the entire observed range of scales, with T and ρ_O being statistically very close to passive scalars. However, ρ_p was quite different, displaying two regimes separated by a characteristic 'planktoscale' typically ~100 m, but highly variable. The large-scale regime was neither passive scalar nor growth dominated (Denman–Platt), but was rather in between the two (the corresponding exponent was $H_p \approx 1/8$ rather than 0 or 1/3, respectively). In addition, we found a new small-scale regime with $H_p \approx -1/3$, which is much 'rougher' than passive scalar (which has $H_p = +1/3$). We propose a simple model involving both growth and turbulence to account for the large scale, and grazing and turbulence (predator–prey zooplankton/phytoplankton interactions) to account for the small scale. Depending on the value of a dimensionless grazing constant $Gr = D/(\tau_g^2\varepsilon)$ (where D is the zooplankton diffusion constant, τ_g is the phytoplankton growth constant and ε is the turbulent energy flux), the small scale is dominated either by the turbulent grazing ($Gr > 1$) or by passive scalar turbulence ($Gr < 1$). In the grazing regime, we also theoretically predict that the density fluctuation exponent = –1/3, which is quite close to the data and quantifies the tendency of the zooplankton to uniformize the phytoplankton distribution by preferentially grazing high-concentration patches.

INTRODUCTION

Ecological scales, levels and wide-range scaling

There is a mushrooming ecological literature on the problem of spatial and temporal scales and its relationship to ecological 'level'; the collections (Powell and Steele, 1995; Peterson and Parker, 1998) contain many recent examples. At first sight, the distinction seems clear enough: scale refers to the spatial extent of an ecological field (such as biomass density, population number density) or to the duration of an ecological process. In contrast, the notion of 'ecological level' refers to a (possibly) corresponding level of 'organization' ('trophic level', 'landscape level', 'canopy level', etc.), and hence to a specific

theoretical framework. Since it is usually assumed that any given ecological process or phenomenon has a relatively well-defined 'characteristic' duration and spatial extent, it is customary to plot the phenomena of interest on a Stommel diagram of the sort shown in Figure 1 [the undoctored basic diagram without the lines is from Steele (Steele, 1995)]. As pointed out by O'Neil and King (O'Neil and King, 1998), it is then common (and problematic) to identify the different phenomena (indicated by the ellipses in Figure 1) with 'levels' and hence with qualitatively different processes and dynamics, each requiring different theoretical models.

The problem with this standard approach goes beyond just the often questionable identification of phenomena with 'level'. It originates in the empirical fact that ecological fields and processes are in fact rarely confined to a narrow range of scales; they typically display structures in time and space over wide ranges of scale. Indeed, the Stommel diagram in Figure 1 shows this graphically for

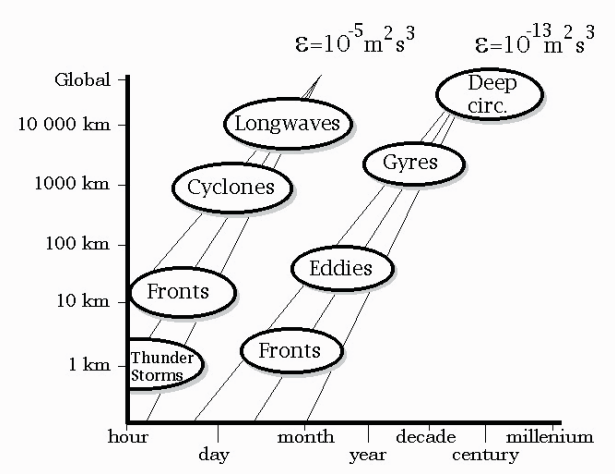

Fig. 1. A Stommel diagram showing the length and time scales associated with typical atmospheric and oceanic dynamics, adapted from Steele (Steele, 1995). Although the original interpretation was in terms of separate dynamical processes at each scale range, the governing equations are in fact scaling over the whole range down to dissipation scales, and at least in the atmosphere [where large amounts of data have now been analyzed, e.g. (Stanway, 2000)] the mean scaling is extremely well respected over the entire dynamically significant range (to at least within 1 or 2% per octave in scale). To show the compatibility of the diagram with the cascade model of wide-range scaling, we have added several straight lines to the original. The thick lines (slope 3/2) are lines of constant energy flux showing that the basic Kolmogorov (non-intermittent) scaling model holds remarkably well for both the ocean and atmosphere. The thin lines give an idea of the fluctuations expected due to multifractal intermittency. Their slopes are $3/(2 + \gamma)$ with singularities γ taken to be $\pm C_1$. When $\gamma = +C_1$ [the left-most thin lines; taken here = 0.25 in accord with atmospheric measurements, e.g. (Schmitt *et al.*, 1992a)] the line indicates the effect of the sparse intermittent structures which give the dominant contribution to the mean. When $\gamma = -C_1$, the thin lines give roughly the space–time relationships for the weaker structures which at any scale are the most probable (when $\alpha = 2$, i.e. for log–normal multifractals, this statement is exact). As expected, the weaker structures live longer at each scale, and the stronger ones less long.

both atmospheric and oceanic dynamics. Processes spanning more than six orders of magnitude of scale are explicitly identified, but the graph could have been extended [see (Schertzer *et al.*, 1997)] down to millimetres and milliseconds (where viscous dissipation finally smooths things out) for a total range of spatial scales of factor nearly 10^{10}.

When examined in the light of turbulence theory and recent advances in scaling notions, the neat classification of structures into 'long waves', 'cyclones', 'fronts', 'gyres', etc. can already be seen to be purely phenomenological. In this approach, phenomena are given different names merely because they appear different; in actual fact, the underlying equations (which are the basic fluid equations) are the same over the entire range. Since the development of sophisticated theoretical frameworks of isotropic homogeneous turbulence in two and three dimensions during the 1960s and 1970s, the key qualitative distinction in dynamical processes in atmospheric and oceanic circulations has been based rather on a somewhat different, but in fact still ultimately phenomenological, classification of flows into 'quasi three-dimensional' (small scale) and 'quasi two-dimensional' (large scale). In this standard model of global circulation, these regimes were then identified with isotropic three-dimensional and isotropic two-dimensional turbulence, respectively. Since such turbulences are fundamentally different from each other (due for example to the absence of vortex stretching in two dimensions), a dimensional transition (Schertzer and Lovejoy, 1985a) or 'meso-scale gap' was postulated to exist separating the small- and large-scale dynamics. However, with the development of generalized scale invariance [GSI (Schertzer and Lovejoy, 1985b)], it became clear that if unique anisotropic dynamical mechanisms repeated scale after scale over wide ranges, they would generally lead to structures with quite different appearances at different scales, but nevertheless ruled by the same dynamic processes throughout. The theoretical basis of the usual phenomenology thus collapsed. Of particular importance was the proposal (Schertzer and Lovejoy, 1985a) that gravity would lead to different horizontal/vertical scaling exponents (e.g. spectral exponents); hence that the turbulence was never isotropic two-dimensional nor isotropic three-dimensional, but rather anisotropic (stratified) 23/9 (~2.555…) dimensional throughout. This prediction has been well confirmed by a series of experiments, most recently in the atmospheric velocity field by Chigirinskaya *et al.* (Chigirinskaya *et al.*, 1994) and Lazarev *et al.* (Lazarev *et al.*, 1994).

If the same mechanism repeats scale after scale in a cascade-like fashion, the resulting structures (geometric sets of points) will be fractals and the resulting fields will be multifractals; the variability will build up scale after

scale from large to small, yielding extreme small-scale variability. What would we then expect to see on a Stommel diagram? In the case of the ocean and atmosphere, thanks to great progress in multifractals and turbulence in the last 15 years, this question can now be answered rather precisely. First, on average, the energy flux ε (units: $m^2\ s^{-3}$) to smaller scales will be conserved scale to scale so that, to a first approximation, all the phenomena will lie on a line of constant slope 3/2 (the thick lines in Figure 1). This is simply dimensional analysis using ε to connect time and space; it corresponds to the Kolmogorov (Kolmogorov, 1941) theory of homogeneous turbulence, the famous Kolmogorov '5/3 power law'. Figure 1 shows that this is indeed already a good approximation if the mean energy fluxes for the atmosphere and oceans are roughly those indicated. However, we can do much better; a recent analysis of nearly 1000 satellite cloud images (Lovejoy *et al.*, 1997, 2000a; Stanway, 2000) gives convincing evidence that the cascades really do start at planetary scales, and that they accurately explain the fluctuation statistics at smaller scales (for both weak and intense phenomena). We can therefore use these and related results on the velocity field to characterize the intermittency/variability that would be generated by the cascade and to determine the spread of the phenomena about the lines; this has been done in Figure 1. Given the arbitrariness of the definitions of scale, structure and phenomena that were used in constructing the undoctored Figure 1, the agreement is surprisingly good. Indeed, the mere fact that all the ellipses lie along roughly a straight line on the log–log plot implies a scaling velocity (a power law function of scale), and hence a single 'organizational level' spanning huge ranges of space–time scales. The resulting interpretation of the Stommel diagram is thus quite different from the usual one. Rather than cataloguing a series of disparate phenomena, each shoe-horned into separate space–time ellipses and each begging to be conceptualized according to different theories or models, the Stommel diagram now graphically demonstrates the unity of a single anisotropic non-linear space–time process repeating scale after scale, building up extraordinary intermittency as it does so. In this wide-range scaling framework, the differences in the phenomena at different space–time scales are simply differences in magnitude (degree of intermittency, anisotropy, strength of interaction with other coupled processes, etc.), not differences in kind.

The example of phytoplankton fields

Perhaps the best documented and best accepted example of wide-range scale in a biological field is the phytoplankton field, which has been studied from scales of millimetres to thousands of kilometres mostly using various proxy measurements, especially fluorescence and ocean colour. In addition, due to the obvious connection between oceanic turbulence and phytoplankton concentration, turbulent scaling methods have been used at least since Denman and Platt (Denman and Platt, 1976) and Denman *et al.* (Denman *et al.*, 1977). Since then, the multifractal cascade picture has been increasingly accepted as a good approximation to fully developed turbulence and has already been used to study phytoplankton (Pascual *et al.*, 1995; Seuront *et al.*, 1996a,b; Claereboudt *et al.*, 2000; Lovejoy *et al.*, 2000b). It is therefore natural to investigate systematically the multifractality of phytoplankton along with other physical variables. This research was one of the motivations of the 3 year Coastal Heterogeneity and Scaling experiment (CHASE) whose goal was to examine fundamental mechanisms responsible for the spatial variations in the structure of the near-shore communities. The region studied [stretches of the St Lawrence (Canada) estuary of differing coastal heterogeneity] is a northern tidal estuary with linear shores periodically broken by zones with varying heterogeneity, where semi-diurnal bidirectional tidal patterns of flow and seasonality predominate. As discussed in recent papers (Seuront *et al.*, 1999; Claereboudt *et al.*, 2000), the physical justification of the multifractal framework is that we expect there exist wide space–time ranges in which the complex non-linear biological–physical interactions are scaling. This leads to a cascading influence of shore heterogeneity on near-shore circulation, patterns of phytoplankton and meroplankton abundance, as well as on the benthic shore communities. The goal of this paper is thus both to quantify the range and type of scaling as well as to provide a theoretical understanding of the basic scaling laws and their limits.

1. DATA DESCRIPTION

Sampling was carried out at various phases of the tidal cycle along five locations of the St Lawrence estuary between the Islands of Bic and the Baie des Petits Méchins, between 27 July and 22 August 1994, 13 July and 31 August 1995, and 1–31 July 1996. At each location, several transects of physical and biological variables were recorded along linear trajectories roughly parallel to the shore with bottom depths varying from 7 to 35 m. Temperature, salinity, light transmission, dissolved oxygen and *in situ* fluorescence were recorded at 4 Hz using a Seatech *in situ* fluorimeter mounted on a SeaBird 25 CTD profiler. The device was towed laterally at 2.5 m depth [in 1995 and 1996, an Optical Plankton Counter (OPC) was coupled to the CTD profiler and collected a continuous record of the zooplankton abundance along the transect; the analysis of these data is discussed elsewhere (Currie *et*

al., 1998)]. The sampling rate combined with the velocity of the towing boat (1.6 m s^{-1}) gave a sampling resolution of ~0.4 m. Transects were 2^{12} (= 4096) data points in length, approximately equal to 1600 m. The fluorimeter was calibrated at the beginning and at the end of the sampling season in several large homogeneous volumes of sea water in which *in situ* fluorescence was measured for 5 min. The chlorophyll *a* content of the water samples was later measured by filtering on GF/F fibreglass filters, extraction by 90% acetone and fluorometry (Strickland and Parsons, 1972).

A summary of the mean characteristics of the 66 boat transects analysed here is given in Table I, and some examples of individual series showing their extreme variability over the range of study are presented in Figures 2, 3a and b. The data are organized according to the bay sampled; the five bays were chosen with size systematically decreasing from Sainte-Flavie (straight-line coast: bay 'width' >>10 km) to Capucins ('width' <1 km). The objective was to see whether this systematically increasing scale of heterogeneity (the scale of a single large coastal irregularity) would influence the heterogeneity of the corresponding biological and physical parameters. The table indicates both the mean values and the variation around the mean. In order to quantify the difference between the different bays, we performed one-way ANOVA and Fisher's protected LSD post hoc tests to group different values, from which we drew several conclusions. Considering the mean values of the fields, there seemed to be three different cases. The Bay of Capucin can be grouped with the Bay des Mechins, which is nearby, and the Bay of Anse au Coques is similar to the Bay of Mitis. This distinction is based mainly on temperature, salinity and turbidity, which implies that the three cases have different water masses (different densities) and different amounts of suspended material (as inferred by the transmission). Light transmission is sensitive to almost all matter in suspension in the water, whereas fluorescence is primarily sensitive to chlorophyll *a*. We shall see that the differences in the means are in fact more pronounced than the differences in the variability (as quantified by the multifractal analyses); this is perhaps not surprising since it simply indicates that the mechanism generating the inhomogeneity is primarily turbulent and is independent of the bay.

2. THE RANGE OF SCALING

2.1 The physical parameters

As usual in scaling analyses, we must first characterize the scaling range and then, within the range, the type of scaling. Since the most sensitive method of detecting scaling and its limits is via the energy (variance) spectrum, we first consider this. Figure 4a and b shows examples of spectra for individual series (using logarithmically spaced spectral averaging intervals to smooth the high-frequency noise), showing that, if only due to the extreme intermittency, single transects are extremely variable, though roughly follow a linear trend on log–log plots as expected for scaling. Since scaling is a statistical symmetry principle, the (high) variability about the power law is the result of intermittency; theoretically, we expected only that the ensemble spectrum would be scaling. An attempt to estimate the ensemble spectra may be obtained by averaging over all the series available for a given bay; this is shown systematically in Figure 5. Here, the fluctuations are sufficiently attenuated so that a clearer picture is obtained.

Before discussing these spectra in more detail, recall that the simplest model for the physical parameters is when they are passively advected by a turbulent velocity (more details are given in Section 2.3). This would lead to a (Corrsin–Obhukov) power law spectrum $E(k) \approx k^{-\beta}$ with spectral exponent $\beta \approx 5/3$ (k is a wave number). Such behaviour is indeed convincingly observed for the temperature spectra (Figure 5b), indicating that the

Table I: Mean values of the measured fields

Bay	No. of samples	ρ	T	ρ_O	S	t
Sainte-Flavie	37	0.364 ± 0.138b	10.10 ± 1.49a	6.86 ± 0.52c	26.32 ± 0.63c	59.11 ± 6.88a
Mechin	11	0.115 ± 0.017a	15.88 ± 0.851a	5.60 ± 0.104a	24.80 ± 0.275c	77.34 ± 1.25
Mitis	13	0.234 ± 0.157a	11.56 ± 1.18a	7.08 ± 0.33c	25.86 ± 0.598b	66.86 ± 11.45b
Anse aux Coques	3	0.247 ± 0.085ab	11.58 ± 0.876a	6.32 ± 0.08b	26.30 ± 0.183bc	65.53 ± 5.90ab
Capucins	2	0.105 ± 0.007a	17.03 ± 0.085a	5.74 ± 0.16ab	24.49 ± 0.007a	77.44 ± 0.77c

The variability about the mean for each bay (corresponding to 1 SD) is shown in parentheses. Different letters correspond to groups with significantly different means according to results of Fisher's protected LSD post hoc test of one-way ANOVA on the mean values of the field. When two letters appear, the results could not be identified as belonging to one group or the other.

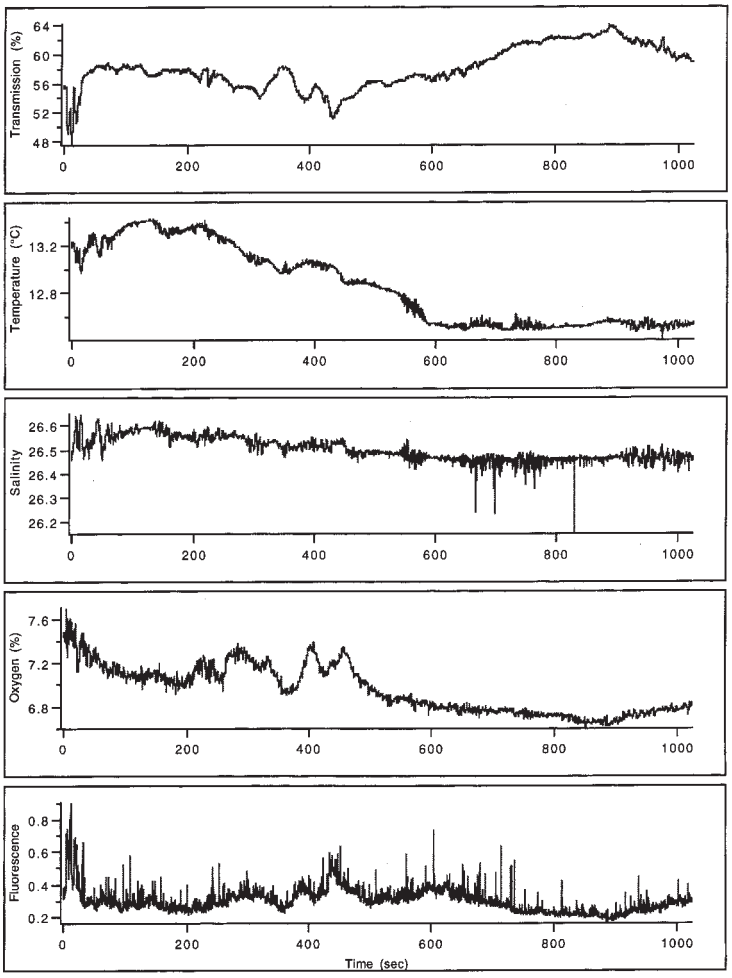

Fig. 2. Example of the raw data taken during a transect with the boat.

turbulence continued down to the smallest observed scales (the peak in the top and third series at ~2–3 s corresponds to the rocking of the boat). Because of its special importance, accuracy of measurement, and the availability of other comparable analyses, we compare in Table IIa the temperature exponents (including the spectral exponents) for the overall average of the 66 series studied here, the 10 subsets considered in Claereboudt *et al.* (Claereboudt *et al.*, 2000), as well as values determined in time (rather than space) in the ocean (Seuront *et al.*, 1996a,b, 1999), as well as for the atmosphere (time and horizontal). We see that our value of β is a little lower than the others (slightly less than 5/3), although it is particularly close to the value obtained by Seuront *et al.* (Seuront *et al.*, 1996a) in the English Channel [an anomalous low-frequency result reported in Seuront *et al.* (Seuront *et al.*, 1999) is discussed in Section 2.4].

Of the other physical fields, only the oxygen spectra (Figure 5c) were similar to this and close to passive scalar values (Table IIIa; overall $\beta_O \approx 1.66$), although for frequencies above ~0.1 Hz there was evidence of both the broad spike in the top and third series (again, the boat rocking), as well as of a more rapid than expected fall-off in the fourth and fifth series, and less rapid fall-off in the second series. This high-frequency behaviour may be an artifact related to a mixing time of ~10 s in the Seabird oxygen probe.

For the salinity, we found reasonably good scaling (Figure 5d), but again with the exception of the broad peak in the top and third series, and a systematic tendency to fall-off more quickly at frequencies >0.1 Hz (again compatible with possible measuring device smoothing). In addition, in Table IIIa, we see that β_S was closer to one; we shall see that, quantitatively, it is not compatible with a passive scalar behaviour. This presumably reflects non-passive salinity buoyancy effects.

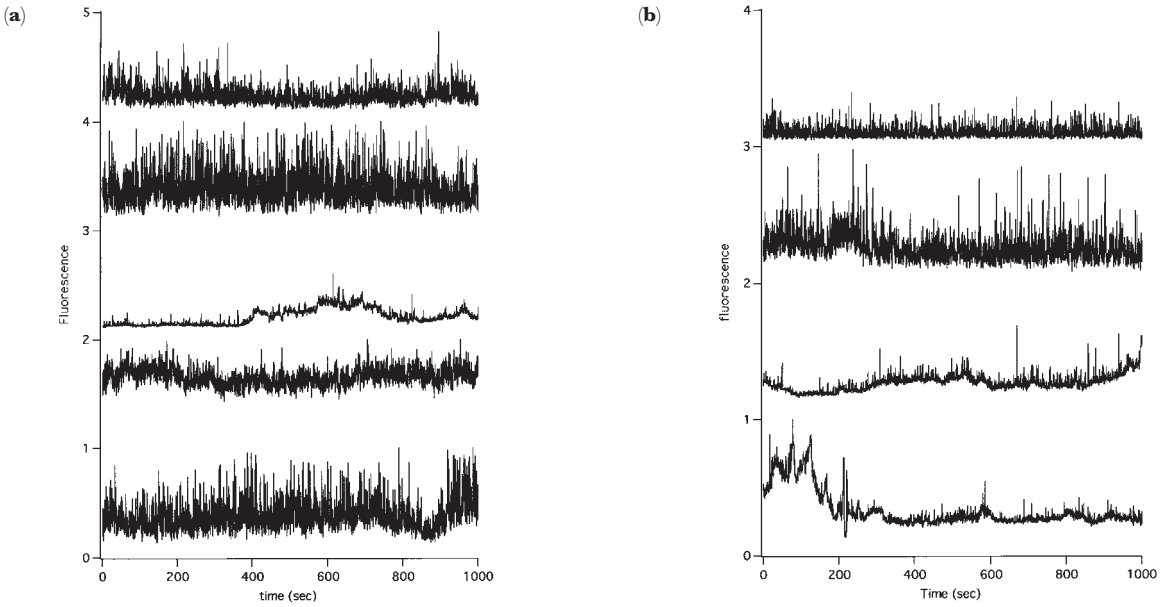

Fig. 3. (**a**) Raw data for fluorescence in a dominant wind of 11 knots and various depths of the water column (graphs are vertically offset for clarity). (**b**) Raw data for fluorescence with a water depth of 15 m and various wind conditions (graphs are vertically offset for clarity).

The physical interpretation of the transmission data is not straightforward. It is the optical transmission through a gap 50 cm wide; hence, it depends non-linearly on the optical density (if we ignore multiple scattering, the dependence is exponential), the latter being in turn non-trivially related to particle density (e.g. it depends on the phytoplankton particle size distribution and extinction cross-sections) as well as on other sources of turbidity present. In any event, it was generally found to have excellent scaling (Figure 5e), although with highly variable exponents. Since the overall average ($\beta_t \approx 1.25$) was not in fact too far from the low-frequency fluorescence value ($\beta_p \approx 1.18$), it is tempting to conclude that it tracks the fluorescence, but detailed comparison shows that while the two are correlated, their relationship is not simple; in particular, the transmission did not show the clear break displayed by the fluorescence data.

2.2 The plankton proxy data

Figure 5a shows the fluorescence spectra for the different bays, indicating a low-frequency regime with $\beta_p \approx 1.18$ (the left-most lines in the figure). Table IIb indicates transect-to-transect deviation in the mean low-frequency exponents, ± 0.1. The break point separating the high- and low-frequency regimes was determined by the intersection of the high- and low-frequency scaling regimes. This is near the mean of the Denman–Platt value 1, and the passive scalar 5/3 value, and is in agreement with the Seuront *et al.* (Seuront *et al.*, 1996a) value $\beta_p \approx 1.22$ found from a time series spanning the frequency range 0.03–10^{-5} Hz (see Table IIb for a detailed comparison and Section 2.3 for a theoretical model). At distances around 100 m (but whose position is highly variable; e.g. in the Les Mechins series there is no clear break, see Figure 5a), there was a break in the scaling with a nearly flat high-frequency regime [the right-most break at the last factor of four at the high-frequency end (>1 Hz) is an artifact due to the time constant of the device of ~1 s]. The plateau region ($\beta_p \approx 0.41$) was not expected and to our knowledge it is the first time it has been observed (for reference, $\beta_p = 0$ is the value for Gaussian white noise). Note that, in contrast, while Seuront *et al.* (Seuront *et al.*, 1996a,b) found a low-frequency regime (0.03 Hz) similar to the one found here, their high-frequency regime was close to the passive scalar value: $\beta_p \approx 1.75$. If we perform a rough time–space conversion, using a typical tidal velocity of 1 m s^{-1}, we find that our break at ~100 m (really, in the region 10–1000 m) is roughly compatible with a spectral break at a frequency of 0.03 Hz, which at this speed corresponds to a spatial scale of ~30 m. However, rather than the break leading to smoother (larger β_p) passive scalar type behaviour, we observed a significantly rougher (lower β_p) behaviour; see the discussion below and Abraham (Abraham, 1998) for a simple model.

Table IIa: Comparison of overall temperature parameters with data for this paper in bold

	C_1	α	H	β	q_D
Ocean					
Space (Claereboudt *et al.*, 2000)	0.044 (0.003)	1.85 (0.01)	0.35 (0.02)	1.62 (0.03)	3.65 (0.15)
Space (this paper)	**0.031 (0.01)**	**1.81 (0.03)**	**0.31 (0.05)**	**1.63 (0.02)**	**4.3**
Time (Seuront *et al.*, 1996a)	0.04	1.70	0.42	1.74	–
Time (Seuront *et al.*, 1996b)	0.037	1.70	0.34	1.65	–
Time[a] (Seuront *et al.*, 1999)	0.050	1.90	0.40	1.72	–
Atmosphere					
Time (Schmitt *et al.*, 1992b)	0.042	1.2 (0.1)	0.40	1.75 (0.05)	3 (1)
Time (Schmitt *et al.*, 1996)	0.04 (0.005)	1.45 (0.05)	0.38	1.70	–
Time (Finn *et al.*, 2000)	0.08	1.68	0.44	1.74	
Time (Wang, 1995)	0.10	1.69	0.41	1.64	
Time (Pelletier, 1995)	0.08	1.69	–	–	
Space (Chigirinskaya *et al.*, 1994)	0.04 (0.01)	1.25 (0.06)	0.33 (0.03)	1.70 (0.05)	5.5

For Claereboudt *et al.* (Claereboudt *et al.*, 2000) and this paper, errors (in parentheses) are interbay average variabilities. The 1 SD variability on the present data is based on the bay means for Claeredeboudt *et al.* (Claeredeboudt *et al.*, 2000) and corresponds to half the difference between the Sainte-Flavie and Mitis values. In the other cases, the cited accuracies were used.
[a]These results are for times <1000 s; the low-frequency results were anomalous and are discussed in Section 2.4.

Table IIb: Fluorescence global comparisons with data for this paper in bold

	C_1	α	H	β
Low frequency				
Space (Claereboudt *et al.*, 2000)	–	–	0.21 (0.06)	1.31 (.13)
Space (this paper)	**–**	**–**	**0.11 (0.05)**	**1.18 (0.1)**
Time (Seuront *et al.*, 1996a)	0.02 (0.01)	0.8 (.02)	0.12	1.22
Time (Seuront *et al.*, 1999)	0.24	1.37	0.66	1.96
High frequency				
Space (Claereboudt *et al.*, 2000)	0.064 (0.05)	1.84 (0.01)	–0.31 (.02)	0.26 (0.03)
Space (this paper)	**0.022 (0.01)**	**1.86 (0.10)**	**–0.27 (0.05)**	**0.41 (0.1)**
Time (Seuront *et al.*, 1996a)	0.04 (0.01)	1.80 (0.05)	0.41	1.75
Time (Seuront *et al.*, 1996b)	0.035	1.80	0.36	1.66
Time[a] (Seuront *et al.*, 1999)	0.06	1.80	0.43	1.77

For Claereboudt *et al.* (Claereboudt *et al.*, 2000) and this paper, standard deviations (parentheses) are interbay average variabilities. The low-frequency C_1 and α values were not estimated due to an inadequate range of scales.
[a]These anomalous results are for times >1000 s; see Section 2.4 for a discussion.

2.3 Recap of passive scalar and growth-dominated patch statistics

The turbulent framework for patch statistics is based on various fluxes; the basic ones being the energy flux ε_l from large to small scales:

$$\varepsilon_l = \frac{\Delta v_l^2}{\tau_{e,l}} \quad (1)$$

and is the variance flux χ_l of passive scalar from large to small scales:

$$\chi_l = \frac{\Delta \rho_l^2}{\tau_{e,l}} \quad (2)$$

the subscript l denotes the scale of the structure, where Δv_l is the typical shear across the eddy and $\Delta \rho_l$ is a typical

gradient of the passive scalar concentration across the eddy. Note that these fluxes are from large to small scales and are only equal to the corresponding dissipation rates at the smallest (dissipation) scales. Whereas $\tau_{p,l}$ is the characteristic lifetime of a structure in the ρ field, $\tau_{e,l}$ is the corresponding characteristic lifetime for a structure in the velocity field (the 'eddy turnover' time). The fluxes χ_l, ε_l are usually considered fundamental since they are exactly conserved by the non-linear terms of the equations of passive scalar advection.

At scales much larger than the viscous scale, $\tau_{e,l}$ is determined only by l and Δv_l, hence (by dimensional analysis):

$$\tau_{e,l} = \frac{l}{\Delta v_l} = l^{2/3} \varepsilon_l^{-1/3} \quad (3)$$

Table IIIa: Values of the mean spectral exponent β

Bay	No. of samples	ρ (low frequency)	ρ (high frequency)	T	ρ_o	S	t
Sainte-Flavie	37	1.14	0.26 ± 0.39b	1.65 ± 0.24a	1.87 ± 0.23b	1.26 ± 0.55a	1.48 ± 0.19c
Mechin	11	0.99	0.99 ± 0.24c	1.65 ± 0.23a	1.51 ± 0.52a	1.05 ± 0.38a	0.56 ± 0.52a
Mitis	13	1.15	0.25 ± 0.21ab	1.63 ± 0.26a	1.67 ± 0.35b	0.96 ± 0.23a	1.14 ± 0.33bc
Anse aux Coques	3	1.07	0.13 ± 0.01a	1.58 ± 0.32a	1.59 ± 0.18b	0.24 ± 0.81a	1.53 ± 0.54ab
Capucins	2	1.57	0.44 ± 0.02bc	1.65 ± 0.07a	1.68 ± 0.68ab	0.76 ± 0.19a	1.52 ± 0.16abc
Overall	66	1.18 (0.1)	0.41 (0.1)	1.63 (0.02)	1.66 (0.1)	0.85 (0.3)	1.25 (0.3)

The value in parentheses (in the bottom row) is an estimate of the SD of the five locations about the overall mean. The accuracies (indicated by '±') correspond to 1 SD variability within the given bay and give an idea of the transect-to-transect variation. Different letters correspond to groups with significantly different means according to results of Fisher's protected LSD post hoc test of one-way ANOVA on the mean values of the field. When two letters appear, the results could not be identified as belonging to one group or the other.

Table IIIb: Values of the mean universal multifractal parameter H

Bay	No. of samples	ρ (low frequency)	ρ (high frequency)	T	ρ_o	S	t
Sainte-Flavie	37	0.09	–0.35 ± 0.20b	0.36 ± 0.12a	0.47 ± 0.12b	0.17 ± 0.28a	0.25 ± 0.10c
Mechin	11	0.01	0.01 ± 0.12c	0.19 ± 0.12a	0.29 ± 0.26a	0.06 ± 0.19a	–0.21 ± 0.26a
Mitis	13	0.10	–0.35 ± 0.11ab	0.34 ± 0.13a	0.37 ± 0.18b	0.03 ± 0.11a	0.08 ± 0.17bc
Anse aux Coques	3	0.07	–0.40 ± 0.01a	0.31 ± 0.16a	0.32 ± 0.09b	–0.35 ± 0.39a	0.27 ± 0.26ab
Capucins	2	0.30	–0.27 ± 0.01bc	0.37 ± 0.04a	0.37 ± 0.32ab	–0.07 ± 0.09a	0.27 ± 0.08abc
Overall	66	0.11 (.05)	–0.27 (0.05)	0.31 (0.05)	0.36 (0.05)	–0.03 (0.1)	0.14 (0.1)

Table IIIc: Values of the mean universal multifractal parameter C_1

Bay	No. of samples	ρ (high frequency)	T	ρ_o	S	t
Sainte-Flavie	37	0.026 ± 0.011b	0.033 ± 0.015a	0.035 ± 0.012ab	0.044 ± 0.018a	0.010 ± 0.017ab
Mechin	11	0.014 ± 0.004a	0.031 ± 0.014a	0.036 ± 0.011ab	0.035 ± 0.016a	0.009 ± 0.001a
Mitis	13	0.026 ± 0.027b	0.032 ± 0.026a	0.036 ± 0.019b	0.053 ± 0.023a	0.010 ± 0.025b
Anse aux Coques	3	0.034 ± 0.002ab	0.018 ± 0.003a	0.027 ± 0.008a	0.031 ± 0.017a	0.010 ± 0.000ab
Capucins	2	0.011 ± 0.001a	0.043 ± 0.002a	0.033 ± 0.023ab	0.049 ± 0.010a	0.009 ± 0.000ab
Overall	66	0.022 (0.01)	0.031 (0.01)	0.034 (0.01)	0.042 (0.01)	0.01 (0.001)

Table IIId: Values of the mean universal multifractal parameter α

Bay	No. of samples	ρ (high frequency)	*T*	ρ_o	*S*	*t*
Sainte-Flavie	37	1.79 ± 0.05a	1.81 ± 0.08a	1.79 ± 0.05ab	1.78 ± 0.10a	1.94 ± 0.06a
Mechin	11	1.92 ± 0.09b	1.81 ± 0.07a	1.84 ± 0.07ab	1.78 ± 0.08a	1.98 ± 0.02ab
Mitis	13	1.80 ± 0.07a	1.79 ± 0.09a	1.84 ± 0.09b	1.92 ± 0.11a	1.95 ± 0.03ab
Anse aux Coques	3	1.79 ± 0.06a	1.75 ± 0.10a	1.76 ± 0.06a	1.87 ± 0.11a	2.04 ± 0.03ab
Capucins	2	2.00 ± 0.10b	1.85 ± 0.08a	1.81 ± 0.07ab	1.92 ± 0.10a	2.03 ± 0.05b
Overall	66	1.86	1.80	1.81	1.85	1.99

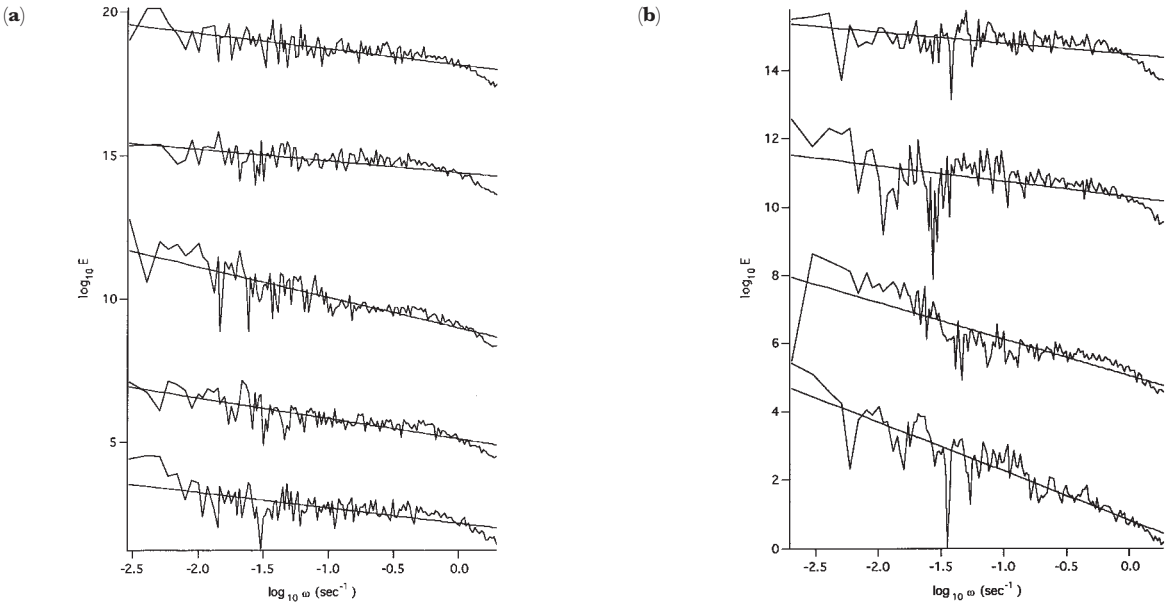

Fig. 4. (**a**) and (**b**) Power spectrum for the flourescence time series of Figure 3a and b, respectively. Note that the instrument resolution is 1 Hz, which accounts for the high-frequency roll-off.

The form of this equation is quite basic; it relates the spatial size and lifetime of a structure via a turbulent flux. It is therefore logical to suppose that a similar form holds for the patch of turbulent scalar (here considered as a possibly 'active scalar'):

$$\tau_{p,l} = \phi_l \, l^{2H_p} \tag{4}$$

where ϕ_l is a flux (not necessarily conserved from one scale to another) that relates the patch size and lifetime. The l exponent ($2H_p$) was chosen since equations (2) and (4) lead to:

$$\Delta\rho_l = \chi_l^{1/2} \phi_l^{1/2} \, l^{H_p} \tag{5}$$

The spectrum of density fluctuations is often used to characterize the statistics. Since the spectrum is the Fourier transform of the autocorrelation (or, for $H_p > 0$, of the structure function: $\left\langle \Delta\rho_l^2 \right\rangle = \left\langle \chi_l \phi_l \right\rangle l^{2H_p}$; see Section 3 for more details), we find the standard result (Monin and Yaglom, 1975):

$$\beta_p = 1 + \delta + 2H_p \tag{6}$$

where the (small) intermittency exponent δ is given by:

$$l^{\delta} = \left\langle \chi_l \phi_l \right\rangle \tag{7}$$

Ignoring the multifractal (intermittent) nature of the fluxes and the possible scaling of their correlation (here,

assuming $\delta = 0$), we can now simply derive the spectral exponents for the two existing models of phytoplankton spectrum: the passive scalar model and the growth-dominated (Denman and Platt, 1976) model. The passive scalar model follows if the patch lifetime is determined purely by the eddy turnover time, i.e.:

$$\tau_{p,l} \approx \tau_{e,l} \tag{8}$$

which leads to $\phi_l = \varepsilon_l^{-1/3}$, $H_p = 1/3$, $\beta_p = 5/3$. On the contrary, following Denman and Platt (Denman and Platt, 1976), if we assume that at least for large enough scales that the patch size–lifetime relationship is governed by a size-independent growth rate τ_g (e.g. the time for exponential doubling of concentrations), then we obtain ϕ_l = constant, $H_p = 0$, $\beta_p = 1$. Alternatively, as we see in the next subsection, we can use the empirical estimate of H_p to specify active turbulence models that account for growth and turbulent mixing as well as the special high-frequency regime.

2.4 A simple theory for the low-frequency phytoplankton exponent: the turbulent growth regime

We saw in the previous section [equation (4)] that the plankton patch lifetime could be expressed in terms of the (generally non-conserved) flux ϕ_l and H_p, which is the (dimensional) non-conservation parameter determining the spatial scaling of the mean plankton concentration fluctuation. Ignoring multifractal intermittency corrections (not so large here since C_{1p} is small; see Table IIIc), we have $\beta_p \approx 1 + 2H_p$; hence, the empirical determination of β_p gives us an estimate of the patch scaling exponent, roughly $H_p \approx 0.1$ (Section 3.1a; see also Table IIb). We see that refined estimates (which include the intermittency corrections) give H_p closer to $0.12 \approx 1/8$, i.e. intermediate with respect to the Denman–Platt value $H_p = 0$ and the passive scalar value $H_p = 1/3$. Since this intermediate regime involves both growth and turbulent dynamics, we call it the 'turbulent growth' regime.

We now show how the empirical value of H_p, combined with dimensional analysis, can be used to obtain a unique low-frequency scaling law. We assume that the low-frequency regime involves both turbulent and plankton growth effects (rather than only one or the other). Dimensionally, we therefore can combine the characteristic growth time τ_g with ε to determine a characteristic turbulent–growth length scale l_g:

$$l_g = \varepsilon^{1/2} \tau_g^{3/2} \tag{9}$$

Using ε in the range 10^{-10}–10^{-14} m^2 s^{-3} (see Figure 1) and $\tau_g \approx 1$ day $\approx 10^5$ s, we obtain l_g in the range 3–300 m. This, combined with τ_g, leads (on purely dimensional grounds) to the following scaling law for the phytoplankon density:

$$\Delta\rho_p = \chi_p^{1/2} \tau_g^{1/2} \left(\frac{l}{l_g}\right)^{H_p} \tag{10}$$

(for simplicity in the following, we suppress the subscripts 'l'). The condition $l > l_g$ is explained below. From this, the patch lifetime is then obtained:

$$\tau_p = \frac{\Delta\rho_p^2}{\chi_p} = \tau_g \left(\frac{l}{l_g}\right)^{2/3} \tag{11}$$

Since the corresponding formula for the turbulent patch scale (the eddy turnover time) is:

$$\tau_e = l^{2/3} \varepsilon^{-1/3} = \tau_g \left(\frac{l}{l_g}\right)^{2/3} \tag{12}$$

we can easily see that for the empirically relevant range $0 < H_p < 1/3$, we have $\tau_p < \tau_e$ for $l > l_g$ and $\tau_p > \tau_e$ for $l < l_g$ so that the turbulent growth regime dominates for $l > l_g$ and the pure turbulence regime for $l < l_g$. We see that the patch lifetime increases with growth rate, but decreases with the level of turbulence (ε). Conversely, for $l < l_g$, the turbulence dominates and we obtain:

$$\Delta\rho_p = \chi_p^{1/2} \varepsilon^{-1/6} l^{1/3} = \chi_p^{1/2} \tau_g^{1/2} \left(\frac{l}{l_g}\right)^{1/3} \tag{13}$$

We thus see that the patch lifetime increases with growth rate, but decreases with the level of turbulence (ε). Using the empirical value $H_p \approx 1/8$, we find:

$$\tau_p = \tau_g^{5/8} \varepsilon^{-1/8} l^{1/4}$$

$$\Delta\rho_p = \chi_p^{1/2} = \tau_g^{5/16} \varepsilon^{-1/16} l^{1/8} \tag{14}$$

Hence, for example, a patch 2^4 times larger will therefore live on average twice as long.

In this model, the large scales $l > l_g$ have both turbulent and growth-determined variability, hence the name 'turbulent–growth' regime. If no other effect is present (and ignoring intermittency corrections), it predicts a high-frequency passive scalar regime with $H_p = 1/3$, $\beta_p = 5/3$, as found by Seuront *et al.* (Seuront *et al.*, 1996a,b) in the English Channel. However, this explanation cannot work here since we find that the high-frequency scaling implies an increased rather than decreased variability with respect to the low-frequency scaling (we find a lower H_p, β_p at smaller scales; see Table IIb). Since the simultaneous temperature records (Figure 5b) show no sign of scaling break (only the $k^{-5/3}$ scaling of turbulence is observed), the breakdown cannot be due to the small-scale dissipation range of the turbulent dynamics (which is typically of the order of millimetres).

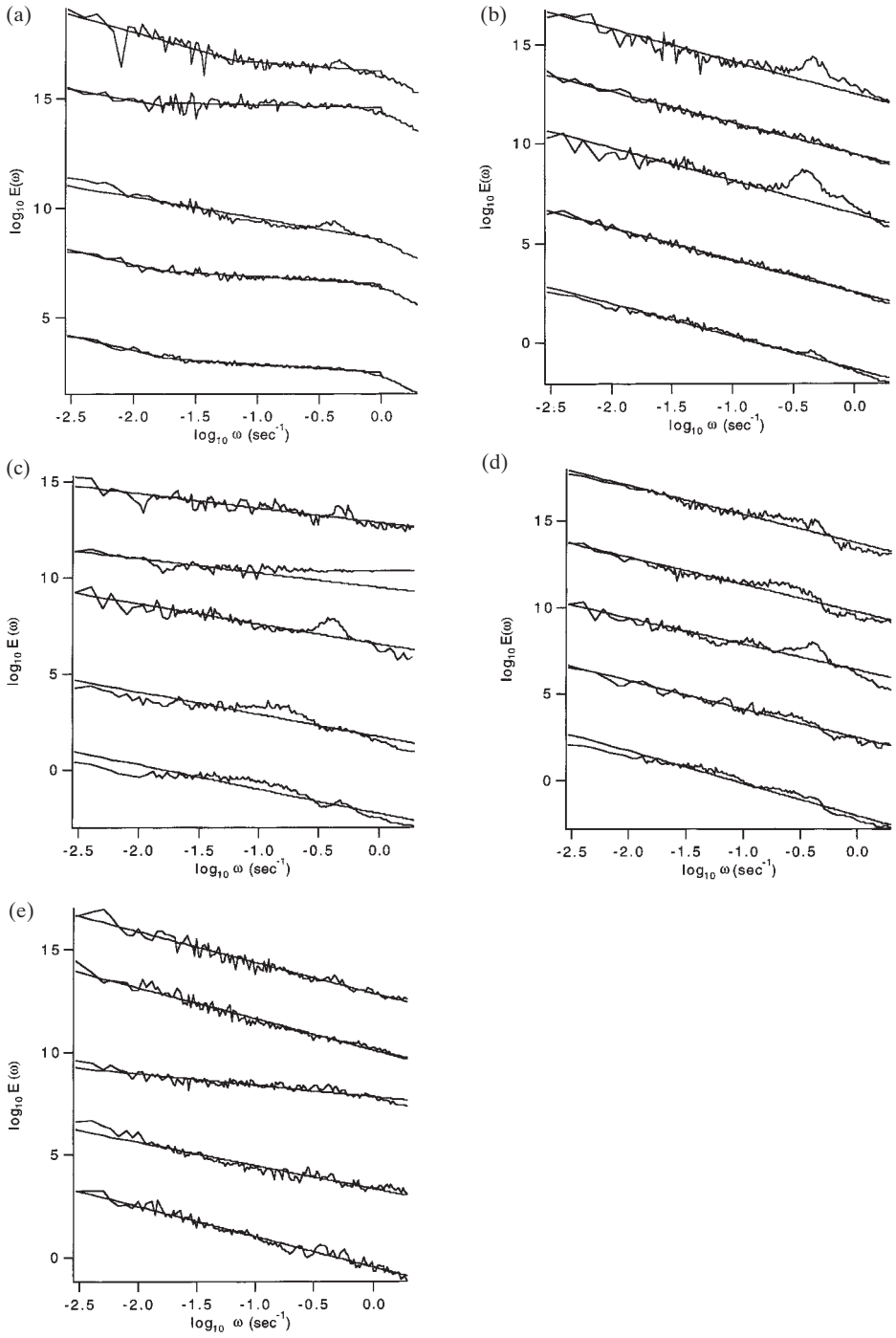

Fig. 5. Average power spectrum (from top to bottom in each case) for the bays Capucins, Anse aux Coques, Mechin, Mitis and Sainte-Flavie. (**a**) Fluorescence; (**b**) temperature; (**c**) oxygen; (**d**) salinity; (**e**) transmission.

Before trying to explain this new high-frequency regime in the next section, we should mention an independent study of ocean colour performed on data taken during the previous summer over a neighbouring part of the estuary (eight visible channels, 7 m resolution). A break in scaling at roughly the same length scale (~100 m) was also observed for chlorophyll-sensitive bands (Lovejoy *et al.*, 2000b). In addition, the large-scale scaling was very similar ($\beta \approx 1.25$; cf. $\beta_p \approx 1.18$) extending up to the extreme large-scale limit of the data (~200 km), showing

that the new turbulent–growth regime spans very wide ranges of scale. The high-frequency regime was also flatter with a lower value of β (~0.4), similar to the high-frequency *in situ* fluorescence found here. The statistical similarity between the two over a range of $>10^4$ in scale provides good support for the use of ocean colour as a phytoplankton proxy. It also indicates that ocean colour–phytoplankton relationships, which had been known to be valid for oceanic water, are also valid for coastal water.

2.5 The planktoscale and the high-wave-number grazing regime

We have seen that the high-wave-number regime had a negative scaling exponent H_p (approximately $-1/3$). Since it would imply that large patches have the shortest lifetime, the classical patch lifetime–size relationship [equation (4)] becomes unphysical. In addition, equation (10) would predict that high levels of turbulence (ε) would make the patches persist longer, another unphysical consequence. We must therefore seek a rather different mechanism. First, consider the implications on the characteristics of the phytoplankton fields. $H_p < 0$ implies that there is a tendency for larger regions to be more uniform than smaller ones (that the density gradients get smaller as the patches get larger). To our knowledge, in the ecological literature, this type of behaviour has only been found in certain numerical models of insect populations [see the discussion in Powell (Powell, 1995)]. This uniformity is only statistical, i.e. the density has sharp small-scale fluctuations that have a tendency to cancel over larger scales. This type of statistical uniformity suggests a disaggregation mechanism resulting from predator–prey or other mechanism (Folt and Burns, 1999). Indeed, since the concentration of phytoplankton is scaling, it is natural to replace traditional patchiness indices [see e.g. (Pinel-Alloul, 1995)], by the parameter H_p, identifying $H_p > 0$ with a tendency for aggregation and $H_p < 0$ for disaggregation. Mathematically, this is justified since $H_p > 0$ means the basic multifractal flux is integrated to yield plankton concentration (fluctuations will tend to accumulate), while $H_p < 0$ implies the converse (differentiation), hence the tendency for fluctuations to cancel. Since the multifractal indices C_1 and α (see Section 3) also affect the patch statistics, they could be regarded as providing refined characterizations of the patchiness.

Direct empirical support for the origin of the break and explanation for the type of scaling was obtained during several transects during the CHASE experiment during 1995 and 1996 [(Currie and Roff unpublished data); Figure 6] when zooplankton were measured by an OPC simultaneously with fluorescence (phytoplankton proxy) measurements. Whenever the turbulent–growth regime was observed in the fluorescence spectrum, the spectrum of the latter, including the scale of the break, was systematically nearly identical to that of the phytoplankton, and this over transects covering the scale range 1 m–16 km long (as compared to 1 m–1 km here). In fact, at every scale, the ratio of the spectral energies (variances) was fairly constant, a fact we will use below. There is evidently a strong non-linear coupling between the zooplankton and phytoplankton populations. In addition, the multifractal exponents C_1 and a were very close to those of the phytoplankton, consistent with a high degree of correlation between their respective concentrations.

In a recent paper (Marguerite *et al.*, 1998), the problem of zooplankton grazing diffusively on a two-dimensional multifractal distribution of phytoplankton was explicitly considered; i.e. a classical diffusion but with extremely variable multi-fractal coefficients was simulated with a classical 'master equation'. The surprising result was that, unlike the one-dimensional analogue (Lovejoy *et al.*, 1998), the diffusion was normal, i.e. the variance of the distance travelled by particles varies linearly with the duration instead of its square for ballistic particle trajectories. This also seems true for higher dimensions, only in dimension one are the particles effectively trapped by high order singularities otherwise they can 'swirl' around them. This implies that for any scale at which the zooplankton's presumably random swimming velocity is greater than the corresponding turbulent velocity, active diffusive grazing can occur. Although this diffusion will be the result of a zooplankton 'random walk', we shall see that it will still be influenced by the turbulence.

To quantify the effect of diffusion, consider the following simple hypothesis that would explain the value of the break scale and the type of high-frequency scaling exponent H. A break, which for obvious reasons we baptized the 'planktoscale' l_d, will appear at the scale where the typical zooplankton diffusing velocity (Δv_z) equals that of the corresponding eddy shear velocity Δv. In this case, the zooplankton can move about at liberty over all scales smaller than or equal to the planktoscale; at larger scales, they are 'prisoners of turbulence', essentially passively advected by these large eddies because their movement rate is insignificant compared to the typical shear velocities across large structures.

To account for the diffusive walk of the zooplankton quantitatively, we must introduce the diffusion constant D (units: $m^2\ s^{-1}$); in the absence of turbulence, the zooplankton displace themselves as:

$$l \approx (D\tau)^{1/2} \tag{15}$$

The corresponding diffusive velocity is:

$$\Delta v_z = D/l \tag{16}$$

i.e. the average velocity decreases linearly with scale. In order to get a rough estimate of D, we can use the order of magnitude estimate that on average zooplankton can travel 1 mm s^{-1} over a distance of 1–10 m. Equation (16) then yields $D \approx 10^{-3}$–10^{-2} m^2 s^{-1}.

The zooplankton will thus be able to overcome the turbulence whenever $\Delta v_z > \Delta v = \varepsilon^{1/3} l^{1/3}$, i.e. for scales $l < l_d$ with:

$$l_d = D^{3/4} \varepsilon^{-1/4} \tag{17}$$

l_d is the diffusion length scale, along with the turbulent growth scale l_g it is the second basic length scale in the problem. In addition, we obtain a diffusion time scale τ_d, which is the typical time for the zooplankton to diffuse to the diffusion scale l_d:

$$\tau_d = \frac{l_d^2}{D} = \left(\frac{D}{\varepsilon}\right)^{1/2} \tag{18}$$

with the pairs l_d, l_g or τ_d, τ_g we can obtain a basic non-dimensional group, which we call the 'grazing number', denoted 'Gr' since it controls the grazing regime:

$$Gr = \frac{D}{\tau_g^2 \varepsilon} = \left(\frac{l_d}{l_g}\right)^{4/3} = \left(\frac{\tau_g}{\tau_g}\right)^2 \tag{19a}$$

For $Gr > 1$, we have $l_d > l_g$; conversely, for $Gr < 1$, $l_d < l_g$.

We have identified three different processes: turbulence, turbulent phytoplankton growth and turbulent zooplankton diffusion. These each have their own time–space relationships; for convenience, we have indicated these in Table IVa. Since at any scale l the dominant process is the fastest (smallest characteristic time), it can be seen that there are three critical lengths and times to consider, corresponding to $\tau_e = \tau_p$, $\tau_e = \tau_{graze}$ and $\tau_p = \tau_{graze}$. The first and second have already been considered, they are τ_g and τ_d, respectively; the last, however, we will denote by the subscripts 'gd' and is given by:

$$l_{gd} = l_g Gr^{1/\left(2\left(1-H_p\right)\right)} = l_d Gr^{1/\left(2\left(1-H_p\right)\right) - 3/4}$$

$$\tau_{gd} = \tau_g Gr^{H_p/\left(1-H_p\right)} = \tau_d Gr^{H_p/\left(1-H_p\right) - 1/2} \tag{19b}$$

Using the empirical estimate $H_p = 1/8$, we obtain:

$$l_{gd} = l_g Gr^{4/7} = l_d Gr^{-5/28}$$

$$\tau_{gd} = \tau_g Gr^{1/7} = \tau_g Gr^{-5/14} \tag{19c}$$

This shows that, for all Gr, $l_g > l_{gd} > l_d$ and $\tau_g > \tau_{gd} > \tau_d$. Figure 7a and b shows the situation graphically for the two cases $Gr > 1$, $Gr < 1$. The figure makes it clear that

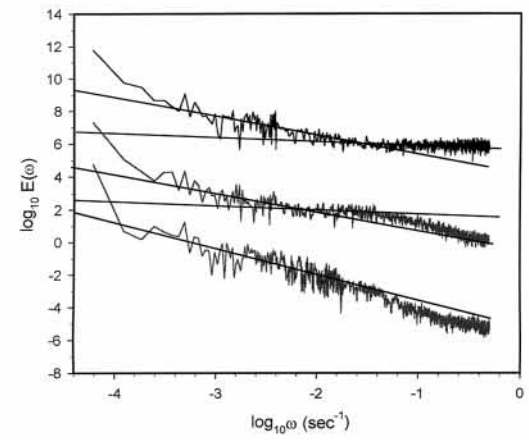

Fig. 6. Spectra of zooplankton biomass estimated from an OPC (top), phytoplankton fluorescence proxy (middle) and temperature (bottom), from Currie and Roff (unpublished data). The reference lines on the plankton curves have the theoretical slopes 1.2 and 0.26, corresponding to turbulent–growth and turbulent–diffusion (grazing) regimes; the temperature spectrum has a reference line of slope 5/3, showing that it is of the form expected for turbulence.

for $Gr > 1$, the relevant transition scale will be l_{gd} rather than l_d since it is the patch lifetime, not the turbulent eddy lifetime, that is critical; we therefore call l_{gd} the 'planktoscale' and τ_{gd} the 'planktotime'. When $Gr < 1$, we see that we obtain a transition to a passive scalar regime of the type found by Seuront *et al.* (Seuront *et al.*, 1996a,b); however, we expect, at small enough scale, zooplankton grazing–diffusion to be dominant.

Using the above estimate of D in the range 10^{-2}–10^{-3} m^2 s^{-1} and ´ in the range 10^{-14}–10^{-10} m^2 s^{-3} with $\tau_g \approx 10^5$, we obtain: $10^{-3} < Gr < 10^2$, which depends sensitively on the level of turbulence (ε), and indicates that both $Gr > 1$ and $Gr < 1$ regimes are likely to be quite common.

We now seek to determine the zooplankton concentration fluctuations for regimes in which grazing is dominant. Similarly to equation (10), dimensional analysis now leads to:

$$\Delta\rho_z = \chi_z^{1/2} \tau_d^{1/2} \left(\frac{l}{l_d}\right)^{H_z} \tag{20}$$

where H_z is the grazing exponent to be determined. As noted above, when $Gr > 1$, the upper limit on the above relationship will be l_{gd}, not l_d. Theoretically, we now see that H_z is uniquely determined if we make the plausible assumption that the only influence of turbulence on zooplankton grazing is via the turbulent shear Δv (rather than via ε or l separately). In this case, we then obtain a unique dimensional result:

$$\Delta\rho_z = \chi_z^{1/2} D^{1/2} \left(\Delta v\right)^{-1} \tag{21}$$

which is the same as equation (20) with $H_z = -1/3$. The

prediction $H_z = -1/3$ is indeed very close to the observed value (see Table II). The real space exponent H_z implies a spectral exponent $\beta_z = 1 + 2H_z - K_z(2)$. If the phytoplankton to zooplankton ratio is indeed roughly constant, then we can use the phytoplankton values as proxies; hence, using the phytoplankton intermittency correction $K_p(2) \approx 0.05$ (see Table IIb), we predict $\beta_z = 0.28$. This is very close to the observed values 0.26 ± 0.03 (Claereboudt *et al.*, 2000) and 0.41 ± 0.1 (Table IIb); the theory is thus close to both empirical estimates. The above turbulent–grazing theory thus predicts that phytoplankton concentration gradients will become progressively smaller at larger scales. This is indeed a plausible result of active grazing since presumably the zooplankton would tend to eliminate local regions of high phytoplankton concentration preferentially. The theoretical form also predicts that if the zooplankton graze faster (larger D), the density becomes 'evened out' faster. Increased levels of turbulent mixing (larger ε) have the opposite effect, presumably making the grazing less efficient. A relevant technical point is that when $H < 0$ the fluctuations at scale l should be characterized by their cross-moments rather than by the structure functions; however, for simplicity of notation, we shall continue to use $\Delta\rho$ for the fluctuation at a given scale.

The main additional hypothesis that we must introduce is that the characteristic fluctuations in zoo- and phytoplankton are in roughly a constant ratio over the entire range from turbulent growth to grazing. This would follow if the ratio of ρ_z/ρ_p was roughly constant, but a less restrictive statistical relationship is all that is required. At least in the cases where $Gr > 1$ [and hence the growth–turbulence ($\beta_p \approx 1.2$) regime was visible], the latter is indeed well supported by the simultaneous measurements of ρ_z and ρ_p by the OPC and fluorescence measurements in CHASE, respectively.

Consider the case $Gr > 1$. To use this observation to extend the phytoplankton statistics to $l < l_d$, with the help of equation (19a), we rewrite the turbulent–growth regime statistics as:

$$\Delta\rho_p = \chi_p^{1/2}\tau_g^{1/2} Gr^{H_p/(2(1-H_p))}\left(\frac{l}{l_{gd}}\right)^{H_p} \qquad l > l_{gd} \quad (22)$$

The behaviour for $l < l_{gd}$ is thus obtained with H_z in place of H_p:

$$\Delta\rho_p = \chi_p^{1/2}\tau_g^{1/2} Gr^{H_p/(2(1-H_p))}\left(\frac{l}{l_{gd}}\right)^{H_z} \qquad l > l_{gd} \quad (23a)$$

Similarly, we may use the same principle (that the fluctuation statistics are in constant ratio) to extrapolate the zooplankton behaviour to larger scales $l > l_{gd}$, obtaining:

$$\Delta\rho_z = \chi_z^{1/2}\tau_d^{1/2}\left(\frac{l}{l_{gd}}\right)^{H_p} Gr^{H_z/(2(1-H_p))-3H_z/4} \qquad l > l_{gd}$$

Finally, we may obtain the ratio of the zooplankton/phytoplankton patch lifetimes for $l > l_{gd}$ as follows:

$$\frac{\tau_z}{\tau_p} = \left(\frac{\Delta\rho_z}{\Delta\rho_p}\right)^2\left(\frac{\chi_p}{\chi_z}\right) = Gr^{(1-3H_p)/2} \quad (24)$$

With a similar approach, we can obtain the corresponding laws for $Gr < 1$; these as well as a comparison of the above results for $Gr > 1$ are shown in Table IVb. A significant feature of the turbulent–grazing regime is that it does not depend on the value of the ratio of the zooplankton to phytoplankton biomass concentrations, it only assumes that the zooplankton actively graze the phytoplankton patches well enough to maintain a roughly constant density ratio.

At small scales, this predator–prey planktoscale model predicts either passive scalar or turbulent–grazing regimes depending only on the value of Gr, not on the biomass concentration ratio; it thus readily explains both our observations and those of Seuront *et al.* (Seuront *et al.*, 1996), primarily by differences in ε. However, other differences in experimental situations are worth mentioning. In particular, the concentration of zooplankton in the English Channel experiment (Seuront *et al.*, 1996) was likely to be low, as inferred from several sources. For example, Baars and Fransz found that (large) copepods grazed only 5% of the phytoplankton standing stock (14% of the primary productivity) per day during the spring (Baars and Fransz, 1984). Smaller copepod stages probably ingested approximately the same amount of chlorophyll *a* per day. Zooplankton densities are significantly lower in spring than they are during summer (Fransz *et al.*, 1984). Several authors have claimed very high zooplankton grazing pressures on phytoplankton: 40% day^{-1} of the standing stocks in Long Island Sound (Capriulo and Carpenter, 1980), and zooplankton grazing matched particulate primary production in the northern North Sea (Daro, 1980). The Channel region shows a typical phytoplankton cycle, with a very strong spring bloom which recedes to low levels during summer and returns with a much smaller subsequent fall bloom (Holligan and Harbour, 1977).

Although the model can plausibly account for the low-frequency ($H_p \approx 1/8$) regime, and even the variation of the high-frequency regime from either $H = -1/3$ or $+1/3$ (depending on Gr), it cannot explain the recent (Seuront *et al.*, 1999) anomalous low-frequency results (see Table IIb). Since the simultaneous low-frequency temperature statistics are nearly identical ($\alpha_T = 0.64$, $C_{1T} = 0.24$, $H_T = 0.64$; see Table IIb for the corresponding fluorescence values), it presumably represents anomalous hydrodynamic

Table IVa: Comparison of the various lifetime–size relationships for the three processes described in the text

Eddy turnover time (turbulence)	$\tau_e = \tau_g \left(\frac{l}{l_g}\right)^{2/3} = \tau_d \left(\frac{l}{l_d}\right)^{2/3}$
Turbulent–phytoplankton growth patch lifetime	$\tau_p = \tau_g \left(\frac{l}{l_g}\right)^{2H_p} = \tau_d \left(\frac{l}{l_d}\right)^{2H_p} Gr^{(3H_p - 1)/2}$
Time required for zooplankton to diffuse/graze region size l	$\tau_{graze} = \tau_g \left(\frac{l}{l_g}\right)^{2} Gr^{-1} = \tau_d \left(\frac{l}{l_d}\right)^{2}$

Table IVb: A comparison of the various high-frequency (small-scale) regimes for both phytoplankton and zooplankton depending on the relative values of the inner growth scale (l_g) and planktoscale (l_d). The non-dimensional grazing number $Gr = (l_g/l_d)^{4/3}$ and, empirically, $H_p \approx 1/8$, $H_z \approx -1/3$

Passive scalar regime: $Gr < 1$; $l_g > l_d$

	Phytoplankton	Zooplankton
Turbulent–growth regime, $l > l_g$	$\Delta\rho_p = \chi_p^{1/2} \tau_g^{1/2} \left(\frac{l}{l_g}\right)^{H_p}$	$\Delta\rho_p = \chi_z^{1/2} \tau_d^{1/2} Gr^{-3H_p/4} \left(\frac{l}{l_g}\right)^{H_p}$
Turbulent regime, $l_{gd} < l < l_g$	$\Delta\rho_p = \chi_p^{1/2} \tau_g^{1/2} \left(\frac{l}{l_g}\right)^{1/3}$	$\Delta\rho_p = \chi_z^{1/2} \tau_d^{1/2} Gr^{-3H_p/4} \left(\frac{l}{l_g}\right)^{1/3}$

Turbulent–grazing regime: $Gr > 1$; $l_d > l_g$

	Phytoplankton	Zooplankton
Turbulent–growth regime, $l > l_{gd}$	$\Delta\rho_p = \chi_z^{1/2} \tau_g^{1/2} Gr^{H_p/(2(1 - H_p))} \left(\frac{l}{l_g}\right)^{H_p}$	$\Delta\rho_p = \chi_z^{1/2} \tau_d^{1/2} \left(\frac{l}{l_{gd}}\right)^{H_p} Gr^{H_z/(2(1 - H_p))} - 3H_z/4$
Turbulent grazing regime, $l < l_{gd}$	$\Delta\rho_p = \chi_p^{1/2} \tau_g^{1/2} Gr^{H_p/(2(1 - H_p))} \left(\frac{l}{l_{gd}}\right)^{H_z}$	$\Delta\rho_z = \chi_z^{1/2} \tau_d^{1/2} \left(\frac{l}{l_{gd}}\right)^{H_p} Gr^{H_z/(2(1 - H_p))} - 3H_z/4$

conditions; indeed Seuront *et al.* speculate that it is the result of frontal mixing, which under certain conditions could theoretically yield $\beta = 2$ for a passive scalar (Seuront *et al.*, 1999). This is justified since their empirical values of β are close to 2 ($\beta_T = 1.98$, $\beta_\rho = 1.96$); note, however, that the theory neglects intermittency (i.e. takes $C_1 = 0$), and hence predicts $H = 1/2$, which is less close to the observed values $H_T = 0.64$, $H_\rho = 0.66$. In any case (some of the following comments apply to some of the early papers by Seuront *et al.*), their study site is in a region known for its complex hydrodynamics. Models produced to predict phytoplankton biomass work fairly well for most of the Channel, but not for the region of the Straits of Dover (Hoch and Ménesguen, 1997). In addition, this is a transition zone with different plankton communities on either side of the Strait (Brylinski *et al.*, 1988). Finally, it could be mentioned that the results of Seuront *et al.* (Seuront *et al.*, 1999) are based on only one time series taken during the spring tide. Spring tides are more likely to produce internal waves and other hydrodynamic effects since the tidal power is much greater during this period (they should have experienced three of these cycles since their transect is >36 h long). In this region of extremely large tidal velocities and vertical mixing, straightforward time–space statistical

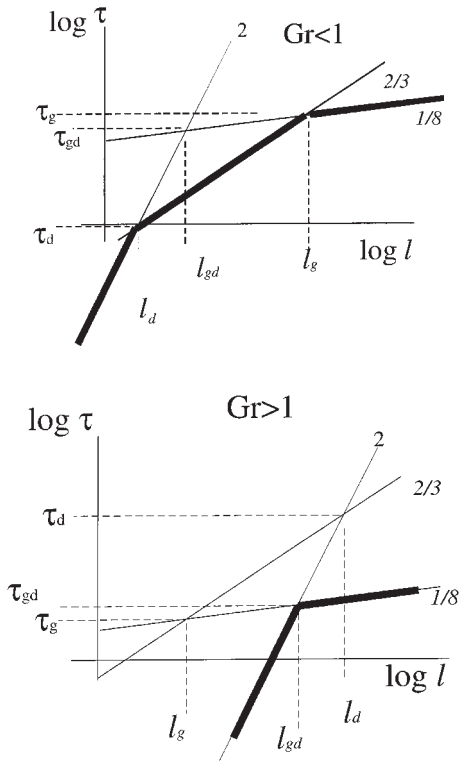

Fig. 7. Schematic diagrams showing the time scales of the various processes which are important in plankton–zooplankton–turbulence interactions. The grazing number *Gr* controls the relative importance of zooplankton turbulent diffusion (identified with grazing) and turbulent growth.

conversions may not be appropriate (or may be rather different in form than those usually assumed for homogeneous turbulence).

The preceding model of active grazing was predicated on the existence of normal zooplankton diffusion (the exponent 1/2 in eq. 15). Indeed, this seems to be the appropriate law in dimensions higher than one if only the multifractal properties of the medium are important (e.g. the multifractal properties of the distribution of phytoplankton for the zooplankton walk). To our knowledge, this exponent has not been directly verified empirically. It is therefore worth pointing out that recent mathematical developments (Schertzer *et al.*, 2000) suggest another possibility for active diffusion generated by Lévy motions, instead of Brownian motions. This is possible since it has been recently shown that the corresponding probability (or concentration) of particles, is solution of a fractional Fokker-Planck equation, i.e. the classical Laplace operator for diffusion is replaced by some of its fractional powers, with possibly non constant coefficients (Schertzer *et al.*, 2000). Its solutions have an interesting and very suggestive phenomenology: the particles follow a series of sticking (pauses), when the particle is trapped (e.g. by high concentration of food), and (fast) flights, when the particle moves (to another cluster of food). These mathematical results may be appropriate if the exponent in eq. 15 turns out to be $\neq 1/2$ and suggest new ways of understanding and studying 'universal' active grazing.

3. TYPES OF SCALING

3.1 Universal multifractal exponents

3.1 (a) The non-conservation parameter H

Analytical approaches to turbulence generally ignore or minimize intermittency; they are 'quasi-normal' and hence are fully characterized by the single exponent H (or, equivalently, by their value of β). However, we must examine systematically all the statistical moments of the fluxes not just the second order (variance as is done in the usual spectrum) in order to characterize the types of scaling fully. This corresponds to an analysis of all levels of intensity. More precisely, we define the scaling moment exponent $K(q)$ by:

Table V: Overall comparison of universal multifractal parameters and q_D (extremes)

	H	C_1	α	q_D
ρ (high frequency)	–0.27	0.022	1.86	3
T	0.31	0.031	1.80	4.3
ρ_O	0.36	0.034	1.81	4.1
S	–0.03	0.042	1.85	4
t	0.14	0.01	1.99	3

The low-frequency fluorescence values are not given since only the value $H_\rho = 0.11$ was estimated due to paucity of low-frequency statistics. Note that T and ρ_O have roughly passive scalar values of H, while the values of C_1, α and q_D are very similar for all parameters except t. The latter has $\alpha \approx 2$, indicating that it may not be universal at all (in which case the C_1 value is the best log–normal approximation).

$$\left\langle \varepsilon_l^q \right\rangle = l^{-K(q)} \tag{25}$$

'< >' indicates 'ensemble average'. If the flux ε_l is conserved scale by scale, then $<\varepsilon_l>$ = constant and $K(1) = 0$. Without further information, the theoretical or empirical characterization of a scaling system would then be impossible; it would amount to the determination of an infinite number of parameters [the entire $K(q)$ function]. In order to make progress, we must restrict $K(q)$ to certain classes characterized by a finite number of parameters. Fortunately, due to the (mathematical) existence of stable, attractive multifractal processes (Schertzer and Lovejoy, 1987, 1997), three basic parameters will generally suffice. H, which measures the degree of (scale-by-scale) non-conservation, has already been mentioned. The other two, a and C_1, characterize the conservative energy flux ε_l:

$$K(q) = \frac{C_1}{\alpha - 1}\left(q^\alpha - q\right) \qquad \alpha \neq 1 \tag{26}$$

$$K(q) = C_1 q \log q \qquad \alpha = 1$$

$0 \leq \alpha \leq 2$ is the Levy index characterizing the degree of multifractality; $\alpha = 0$ corresponding to the monofractal [linear $K(q)$] 'beta model', while the limit $\alpha = 2$ is the 'log–normal' multifractal [although, as indicated below, this is a misnomer since the behaviour in equation (26) generally breaks down for large enough q due to 'multifractal phase transitions' associated with self-organized critical behaviour of the extremes].

Finally, the C_1 parameter is the 'co-dimension of the mean', i.e. it is the co-dimension of the set of points which give the dominant contribution to the mean of the conserved flux. The corresponding fractal dimension is equal to $d - C_1$, where d denotes the standard dimension of space. A large C_1 corresponds to a very sparse process implying that most of the activity contributing to the mean behaviour is extremely violent, but confined to a very sparse set (low fractal dimension). Conversely, a low C_1 implies a more uniform, less extreme process. For example, Gaussian white noise is statistically uniform and has $C_1 = 0$; hence it is space filling.

For universal multifractals, the characterization of the type of scaling amounts to the determination of H, C_1 and α. As discussed in Seuront *et al.* (Seuront *et al.*, 1999) and Claereboudt *et al.* (Claereboudt *et al.*, 2000), it is convenient to use the 'double trace moment' (DTM, which is discussed in detail in the next subsection) technique for this, estimating the universal multifractal parameters C_1 and α. From the derived value of $K(2)$, and the spectral exponent β, we estimate $H = [\beta + K(2) - 1]/2$. Together, the three universal multifractal parameters determine the structure functions and hence statistics at all scales and intensities/moments.

H is empirically determined from the spectral slope β and the DTM estimates of α and C_1. Since here we find that the value of C_1 [hence $K(2)$] is small, the differences in H mainly reflect differences in the spectral slopes. Table IIIb presents the different values of H that were obtained. As noted earlier, the temperature and oxygen series had β close to 5/3; we see that the corresponding H values are in the vicinity of 1/3, which is the theoretical dimensional value for a passive scalar. Table IIa indicates that our horizontal transects in the Gulf of St Lawrence are close to the observed ocean temporal values as well as to both the temporal and horizontal spatial values in the atmosphere.

Similarly, the low-frequency fluorescence and transmission are similar to each other, varying significantly from bay to bay but generally in the same way, with an overall value $H_\rho \approx 1/8$ intermediate to the passive scalar and Denman–Platt values (5/3 and 0, respectively). In contrast, the salinity is nearly conservative (overall, $H_S \approx 0$).

In order to see whether there were systematic bay-to-bay relationships, we attempted one-way ANOVA tests and used a Fisher's protected LSD post hoc test to group the different values (Table IIIb). From the resulting groupings, we conclude that the variables with a purely physical origin (salinity and temperature) show no dependence on the location, but that the variables with some biological character (fluorescence, oxygen and transmission) show some location dependence. We see that fluorescence and oxygen content are grouped similarly, but that transmission behaves a bit differently. In fact, for transmission, the very large bay (Sainte-Flavie) is the only distinctive case. We found no relationship of this dependency to any of the other measured properties of the bays.

3.1 (b) α, C_1

The difficulty with testing the universality hypothesis and estimating the multifractal exponents α and C_1 is that the universal form [equation (14)] is a non-linear function of q. A simple way of obtaining direct, robust parameter estimates is to use a method called DTM which introduces a second power η in addition to q:

$$\left\langle \left(\varepsilon_L^\eta \right)_l^q \right\rangle = l^{-K(q,\eta)} \tag{27}$$

The notation indicates that the multifractal at the finest resolution L is first raised to the η power, then the resulting field is degraded in resolution to a scale l, and then the q power is averaged over all the available data (in order to estimate the ensemble average). The double-indexed exponent $K(q,\eta)$ is related to the single-indexed one by:

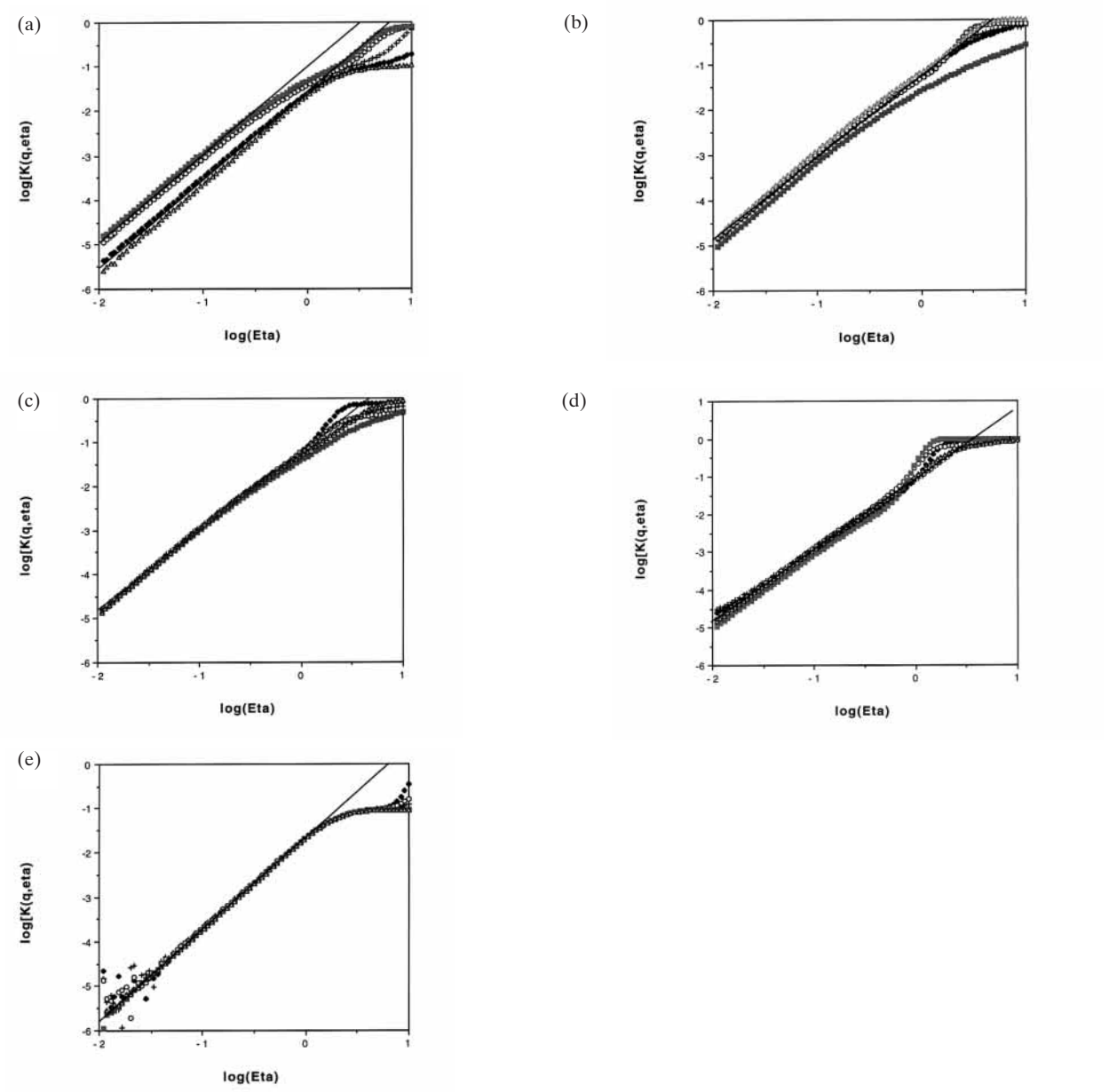

Fig. 8. Log_{10} K versus $\log_{10}$ η; statistics accumulated for 37 series in Sainte-Flavie (crosses), 17 series in Mechin (diamonds), 13 series in Mitis (circles), three series in Anse aux Coques (squares) and two series in Capucins (triangles). (**a**) Fluorescence; (**b**) temperature; (**c**) oxygen; (**d**) salinity; (**e**) transmission.

$$K(q,\eta) = K(q\eta,1) - qK(\eta,1);\ K(q,1) = K(q) \qquad (28)$$

The advantage of the DTM is that when $K(q)$ is of the universal multifractal form, then we obtain:

$$K(q,\eta) = \eta^{\alpha}K(q,1) \qquad (29)$$

[substitute equation (26) into (28)], i.e. a pure power law with respect to η. Using DTMs we estimated the multifractal exponents α and C_1. The $\log_{10}$ K versus $\log_{10}$ η curves are shown in Figure 8a–e. We can see that all the curves fall nearly on top of one another, indicating that they are compatible with production by the same basic multifractal processes irrespective of location. We also can see that they all show reasonably straight sections, indicating $K(q,\eta) = \eta^{\alpha}K(q,1)$, as predicted by the universality hypothesis [the roll-off at large h is a sampling effect/multifractal phase transition as discussed in Schertzer *et al.* (Schertzer *et al.*, 1993)]. Actually, the DTM determines the leading (generally non-integer)

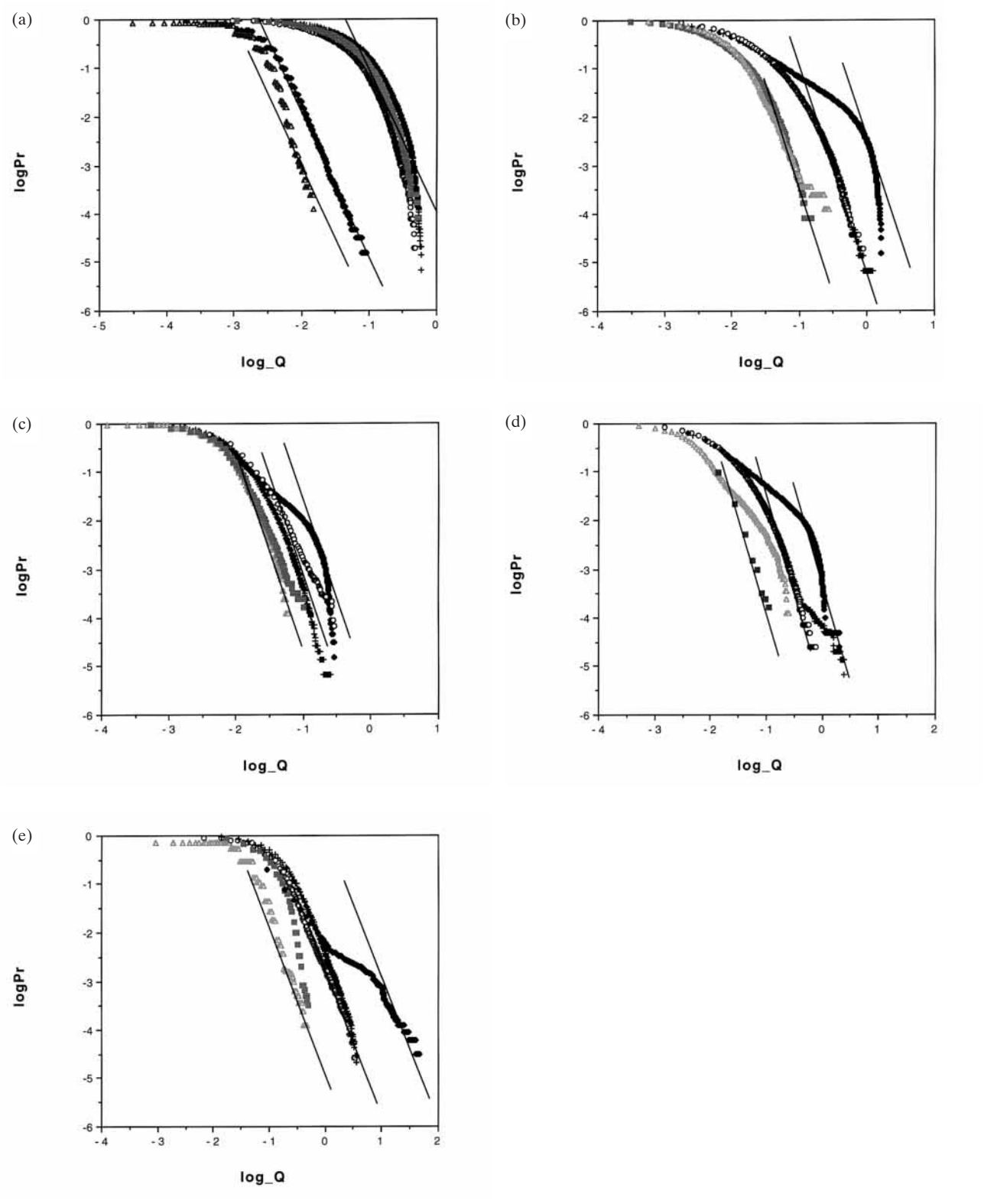

Fig. 9. $\mathrm{Log}_{10}\, Pr\,(x > Q)$ versus $\log_{10} Q$, where Q is an increment threshold; x is a random increment for series from the following bays: Sainte-Flavie (crosses), Mechin (diamonds), Mitis (circles), Anse aux Coques (squares) and Capucins (triangles). (**a**) Fluorescence; (**b**) temperature; (**c**) oxygen; (**d**) salinity; (**e**) transmission.

order of power law expansion of $K(q)$ near $q = 0$ with the linear term removed. Since universality predicts such a generally non-integer order of non-analyticity (i.e. q^α behaviour, a non-integer), it supports the latter when, as here for ρ, ρ_O, S, T, we obtain non-integer a (consistently near 1.8; see Tables IIId and V). However, in the case of t, which is not the direct result of a multifractal process, but rather a non-linear transformation of such a process (e.g. a multifractal biomass density), we obtain a value $\alpha \approx 2$. This result simply means that $K(q)$ is analytic at $q = 0$; since a log–normal yields a pure quadratic $K(q)$, the resulting C_1 gives the best log–normal approximation. Table V compares the overall estimates of the basic multifractal parameters, showing that with the exception of the parameter H they are all fairly close to each other, probably compatible with $C_1 \approx 0.03$, $\alpha \approx 1.8$, $q_D \approx 4$ (see below). If it is true that the main difference between the fields are their H parameters, then this may reflect the dominant influence of the dynamic velocity cascade on all of them, and joint modelling may be particularly simple.

The ANOVA analyses indicate that there are apparently two groups of bay-to-bay variability in fluorescence series: the first for the bays with a more inland character (Sainte-Flavie, Mitis and Anse aux Coques) and the second for ones with a more oceanic nature (Mechins and the nearby Bay of Capucins). The results are reported in Table IIIc and d. Although two groups were identified by Fisher's test (95%) on one-way ANOVA for oxygen and salinity, upon closer examination (Figure 8c and d) we see that these cannot be taken too seriously since Anse aux Coques and Capucins had very few points, and if we eliminate them only one group remains. The same could be said for C_1, considering also that the differences in Sainte-Flavie and Mitis are due mainly to a few outliers. This is clearly seen in differing histograms in Figure 9, in which the outliers are the values at the extreme right-hand side of the distributions. Note that the large-scale fluorescence was not used to estimate C_1 and α values since the scaling regime was too limited for reliable estimates.

3.2 The extremes

A generic feature of cascade processes (Schertzer *et al.*, 1993; Schertzer and Lovejoy, 1994) is that they have frequent extreme events characterized by non-classical (algebraic) statistical distributions of the form:

$$Pr(x > Q) \approx Q^{-q_D} \quad (30)$$

where x is the random variable and Q the threshold; here we take x as the first difference of the series to consider fluctuations. The extreme events giving rise to the probability tails are associated with self-organized critical structures and multifractal phase transitions.

A basic difficulty is that although theory shows that for $a \geq 1$ the multifractals are unconditionally 'hard', i.e. necessarily have finite values of q_D, in practice the value of q_D may be so large that extremely large sample sizes would be required for its determination. A precise criterion for a reliable determination of q_D (i.e. that our sample size is large enough) is $q_s > q_D$, where q_s is the critical 'sampling moment'. As discussed in Schertzer and Lovejoy (Schertzer and Lovejoy, 1994), for universal multifractals, we have $q_s = [(D + D_s)/C_1]^{1/\alpha}$, where D is the dimension of space–time (= 1 here) and D_s is the sampling dimension (= $\log N_s/\log\lambda$, where N_s is the number of transects and λ is the scale ratio in the scaling range). Overall, using the measured values of C_1 and α, we obtain (depending on the bay) q_s in the range 7–11, 6–11, 7–8, 5–8 and 10–13 for (high-frequency) ρ, T, ρ_O, S and t, respectively. These values of q_s (obtained by pooling all the samples from a given bay in order to increase N_s and hence q_s) indicate that any hints of linear asymptotes on log–log (cumulative) histograms (Figure 9a–e) are not statistically significant if their absolute slopes are steeper than these values, i.e. ~5–7. Note that as for C_1 and α, no attempt was made to estimate q_D for the low-frequency fluorescence regime due to inadequate sample size.

Overall examination of the distributions in Figure 9a–e shows that the histograms from bays with the weaker variability (i.e. those to the left) are plausibly asymptotically straight, while those with overall stronger variability are generally asymptotically curved. This curvature could easily be produced by saturation problems with the sensors [recall that we are discussing a possible non-linear measuring problem with the extreme (typically 0.1% of the data)]. Rather than perform systematic regressions to the tail region, we rather show reference lines that typically are fairly accurate for the curves to the left where saturation should not be important. The reference lines have absolute slopes (q_D) values of 3, 4.3, 4.1, 4 and 3 for (high-frequency) ρ, T, ρ_O, S and t, respectively (all these are significantly $< q_s$). These values are close to q_D estimates made for various turbulent passive scalar quantities in the atmosphere [e.g. for pollution (Salvadori *et al.*, 1992), CO_2 (Austin *et al.*, 1991) and tracer gases (Visvanathan *et al.*, 1991) $q_D \approx 3$, 5 and 5, respectively], as well as $q_D \approx 5$ for temperature (see Table IIa). However plausible these results may be, these extreme events are clearly difficult to measure properly and they are by no means conclusive.

4. ANALYSIS OF INDIVIDUAL TRANSECTS

4.1 Possible influence of wind and depth

We have seen that there were no strong systematic bay-to-bay differences in scaling parameters for any of the fields (of course, this does not exclude differences between the mean levels—or even between the amplitudes of the fluctuations at a given reference scale—we only investigated the exponents). It is, however, of interest to examine other possible systematic effects, the most obvious ones being due to the action of wind or to differences in depth. The wind conditions affect the distribution/spectrum of waves and their intensities, while the depth of the water column below the surface modifies the latter via wave dispersion. However, due to the strong (probably scaling) ocean stratification, we do not expect a characteristic depth to imply the existence of characteristic horizontal structures at the same scale only in the horizontal; the 'corresponding' scale will probably be much larger. The standard theory of wind generation of waves is that the wave spectrum $E(k)$ has a maximum corresponding to a wave velocity equal to the wind velocity. This maximum therefore moves to smaller k as the wind increases [this mechanism was described by Shuleykin (Shuleykin, 1956)]. In strong winds (of greater intensity than we experienced since we avoided sampling in these conditions), wave energy is dissipated primarily by white capping. Tessier *et al.* used far-red imagery to confirm that under these strong wind conditions a break/spectral maximum occurs in the range 20–50 m (Tessier *et al.*, 1993). Since the physical parameters had relatively good scaling in all observed conditions (this is particularly true of the temperature, which should be a good indicator of the turbulent dynamics), the effect of such wind-associated breaks cannot be very strong and need only be sought in the plankton proxy. If the wind forcing somehow strongly affects the plankton behaviour, it might influence the observed break.

In order to check the possible influence of both depth and wind, we selected two subsets of our database. The first one consisted of records taken under similar wind conditions, but with various water column depths. The series are shown in Figure 3. At first glance, the variability seems to follow pretty similar patterns. This is indeed confirmed by the spectral analyses shown in Figure 4a. In this figure, we can see that although there is some variation in the spectral slopes, there is no systematic variation in the spectral slopes or in the position of possible positions of scaling breaks with depth. In Figure 4b, we show various transects with the same depth of water below the ship, but with varying wind conditions. In this case, we can see that as the wind increases there is a corresponding increase in the variability in the fluorescence spectrum. The spectral slopes (Figure 4b) become somewhat flatter and the position of a possible scaling break seems to shift toward low frequencies. However, four series are not much data upon which to argue the existence of a relationship. Finally, for all the transects, scattergrams of wind versus β failed to show a strong connection between the two.

4.2 Interrelationships between fields

The standard method of investigating the scale-by-scale interrelationships between the different fields is to use correlation analysis. The difficulty with this for scaling fields is that the result, including even the sign of the correlations, will in general depend on the (subjective) resolution of the measurements. Once again, we require scaling exponents characterizing the interrelationships; the appropriate framework is Lie cascades (Schertzer and Lovejoy, 1995). Work on these did progress during the project; we are currently testing out new numerical simulation and data analysis techniques. However, the main application of this to the data was to use a special case called complex Lie analysis on the temperature/fluorescence series. This did indeed show a scaling interrelationship, but was not adequate for its full characterization.

A more limited semi-empirical examination of the interrelationships was possible by examining the statistical variations of exponent estimates from series to series. We therefore performed one-way ANOVA and Fisher's protected LSD post hoc tests to group different values.

Turning our attention to the scale-by-scale variability as characterized by (α, C_1), using Fisher's test (95%) on one-way ANOVA we did not find convincing groupings; the data were compatible with random statistical variability. Only for the non-conservation parameter H did we see a possible relationship between temperature and salinity. The existence of such relationships between the variability of temperature and salinity is unsurprising since together they specify the density of water mass and hence affect buoyancy.

Although the mean fields were different for different locations (see Section 1 and Table I), the results show very little influence of the coast on the variability, except with a possible distinction between upper estuarine and oceanic connected bays on the variability of phytoplankton. The variability observed is apparently compatible with a pure effect of turbulence.

As we have indicated, the type of scaling is pretty much site independent; this is supported by Figures 5 and 9 and Tables II and III. In fluorescence, however, a slight but significant difference is observed between oceanic and more upper estuarine bays. This can be seen in Figure 5a

and in the log K versus log η curves (Figure 8) show two definite groupings. This is also reflected in Tables II and III, where we see some difference in α and C_1 between the two groups. For the other fields, no such difference is evident.

CONCLUSION

There is a long tradition in ecology of performing phenomenological classifications based primarily on the space–time scales and appearance of phenomena. These classifications typically provide the motivation for the development of a series of distinct models for each scale range and phenomenon type. However, theoretical developments starting in turbulence have shown that when simple dynamical mechanisms repeat scale after scale they build up huge variability. In addition, and this is seldom appreciated, since the dynamics are typically anisotropic, the appearances/morphologies of structures will systematically change with scale even though the dynamics themselves are qualitatively the same over potentially very wide scale ranges (they have no characteristic size). One of the pillars of phenomenology is therefore removed. Since it is apparently sufficient that the (complex, non-linear) dynamics respect very general scale-invariant symmetries, it is now natural to replace the phenomenological approach with a unified scale-invariant one.

We reinterpreted a standard Stommel diagram for the atmospheric and oceanic dynamics, in this unified scaling way showing that it implied the existence of a scaling velocity field, and that the variability was in fact close to that predicted by cascade models. The basic consequence of such scale-invariant behaviour is multifractal statistics; these in turn are predicted to belong to certain 'universality classes', which are stable, attractive behaviours that result when the basic dynamical mechanism is repeated scale after scale. In addition, generic properties of such processes include multifractal phase transitions associated with the appearance of huge (non-classical) extreme variability. These predicted behaviours are quantitatively testable; in this paper (following others), we examine phytoplankton proxy data (fluorescence) and, simultaneously, other physical variables showing that they are indeed compatible with the predictions of the unified scaling framework.

We investigated the effects of coastal heterogeneity on the variability of *in situ*, high-resolution (~1 m) salinity (S), oxygen (ρ_O), temperature (T), optical transmissivity (t) and plankton proxy data (fluorescence; ρ_p). We sought to characterize statistically the heterogeneity of these variables over as wide a range of scales as possible (0.4 m–1.6 km), determining both the range and types of scaling, as well as their scale-by-scale interrelationships. By comparing the characteristics of various bays with systematically varying large-scale heterogeneity, we were able to investigate the influence of the latter on the former.

Discounting occasional spectral peaks due to boat rocking and problems due to instrumental time constants, the basic physical parameters T, ρ_O, S and t were all found to be reasonably scaling over the observed range. The most parsimonious model for explaining these parameters is that the corresponding fields are passively advected by turbulence. This would lead to a (Corrsin–Obhukov) power law spectrum $E(k) \approx k^{-\beta}$ with spectral exponent $\beta \approx 5/3$ and wave number k. Only temperature (T) and oxygen (ρ_O) showed this behaviour. For salinity, β was closer to one; it was found to be nearly a conservative multifractal. The transmission (which non-linearly depends on biomass) had a behaviour close to the low-frequency ρ behaviour.

In contrast, the phytoplankton proxy data showed different low- and high-frequency scaling regimes separated by a 'planktoscale' which was at roughly 100 m in scale, but which in fact varied greatly from case to case. The low-frequency regime was nearly identical to that found by Seuront *et al.* (Seuront *et al.*, 1996) in the English Channel from a single (long) time series; it is in between the passive scalar (turbulent)-dominated regime and a growth-dominated (Denman–Platt) regime. We produced a new hybrid model in which the behaviour (exponent $H_p \approx 1/8$ rather than 1/3 or 0) depends on the non-linear interaction of both turbulent mixing and growth, i.e. in which fluctuations in growth are influenced by turbulence. If no other effects are present, the model predicts that at small enough scales ($l_g = \varepsilon^{1/2}\tau_g^{3/2}$) turbulence will dominate the growth and passive scalar behaviour will result, as found for example by Seuront *et al.* (Seuront *et al.*, 1996).

However, we found quite different small-scale behaviour: rather than a passive scalar regime ($H_p \approx +1/3$), we found much higher variability with $H_p \approx -1/3$; to our knowledge, it is the first time it has been observed. The basic clue to understanding this was the simultaneous observation (using an OPC) that zooplankton biomass had virtually identical spectra to the phytoplankton proxies. Presumably, the zooplankton were actively grazing the phytoplankton by diffusing (performing random walks). Since the mean diffusive velocity decreases linearly with scale and the corresponding turbulent shear grows with scale, at scales larger than the critical scale $l_d = D^{3/4}\varepsilon^{-1/4}$, the turbulence becomes dominant. This means that the plankton can move about at liberty over all scales $\leq l_d$; at larger scales, they are prisoners advected around by the large structures. Since there are two length scales, there is a dimensionless group $Gr = D/(\tau_g^2\varepsilon)$ which controls the grazing and which sensitively

depends on the level of turbulence ε. Whenever $Gr > 1$, we expect that the grazing regime will be dominant at a critical 'planktoscale' l_{gd} with $l_g < l_{gd} < l_d$, where the turbulent diffusion time for the zooplankton equals the turbulent–growth phytoplankton patch lifetime. For $Gr < 1$, the passive scalar regime will be dominant in the range $l_d < l_{gd} < l_g$; below l_d, the grazing (turbulent–diffusion) mechanism is dominant. Finally, in the grazing regime, if we assume that the zooplankton are only influenced by turbulent shear velocity, then dimensional analysis allowed us to determine the unique exponent $H_z = -1/3$, which is indeed very close to the observations.

Concerning the sensitivity of our results to external boundary conditions such as coastal heterogeneity, wind and depth, perhaps the most significant conclusion was that there was no obvious effect of the bay size/type on the range of scaling (we examine the nature of the scaling below). This is perhaps not surprising since the detailed external boundary conditions are not expected to affect a turbulent regime significantly. We also investigated whether other external conditions, such as the surface wind or the depth of the water column, affect the spectra since these would at least affect surface wave spectra. Although there is some evidence of an effect of wind on the spectral slope, the effect was small.

In order to characterize the types of scaling, we must examine systematically all the levels of intensity, i.e. all the statistical moments not just the second (variance) as in the usual spectrum. We primarily used the DTM technique for this, estimating the three universal multifractal parameters (H, C_1 and α) that determine the co-dimension function and the statistics at all scales. As expected, the temperature records indicate H in the vicinity of 1/3, which is (approximately) the value expected for a passive scalar. The transmission, oxygen concentration and low-frequency fluorescence are also close to this value, but not the salinity.

We found that the variables with purely physical origins (salinity and temperature) show no significant dependence on the measurement location, but that the variables with some biological significance (fluorescence, oxygen and transmission) show some location dependence. However, these conclusions are sensitive to the small number of samples from Anse aux Coques and Capucins. We found that fluorescence and oxygen content are grouped together, but that transmission behaves differently (the nearly straight coast case, Sainte-Flavie, is the only exception).

A generic feature of cascade processes is that they have frequent extreme events characterized by non-classical (algebraic) statistical distributions of the form: $\log Pr(x > Q) \approx Q^{-q_D}$ (where x is the random variable and Q the threshold). These are associated with self-organized critical structures and multifractal phase transitions. Using log–log plots, we found (although instrumental problems were noted, primarily slow response time, but also saturation of the phytoplankton proxy signal) for all series that q_D was near four, which is comparable to the results reported elsewhere for temperature. Once again, this may be a typical feature of passive scalar fluctuations.

The standard method of investigating the scale-by-scale interrelationships between the different fields is to use correlation analysis. The difficulty with this for scaling fields is that the result, including even the sign of the correlations, will in general depend on the (subjective) resolution of the measurements. Once again, we require scaling exponents characterizing the interrelationships; the appropriate framework is Lie cascades. Work on these did progress during the project; we are currently testing out new numerical simulation and data analysis techniques. However, the main application of this to the data was to use a special case called complex Lie analysis on the temperature/fluorescence series. This did indeed show a scaling interrelationship, but was not adequate for its full characterization.

A more limited semi-empirical examination of the interrelationships was possible by examining the statistical variations of exponent estimates from series to series. Two quite different cases appeared during comparison of the mean multifractal parameters (Table IIa). The Bay of Capucin should be grouped with the nearby Bay of des Mechins (of more oceanic origin). Anse aux Coques is similar to the neighbouring Bay of Mitis (more upper estuarine). This distinction is based mainly on temperature, salinity and turbidity, implying that the three regions have different water masses (different densities) and different amounts of suspended material (as inferred by the transmission). Transmission is sensitive to almost all matter in suspension in the water, whereas fluorescence is sensitive primarily to chlorophyll. Sainte Flavie seems to lie somewhere between these two cases.

Although the mean fields were different for different locations, the results show very little influence of the coast on variability, except with a possible distinction between more estuarine and oceanic bays on the variability of phytoplankton. When we examined the scale-by-scale variability as characterized by a and C_1 (Table IIIc and d) using Fisher's test (95%) on one-way ANOVA we did not find convincing groupings; the data were compatible with random statistical variability. Only for the non-conservation parameter H did we see a possible relationship between temperature and salinity and bay location (Table IIIb). The existence of such relationships between temperature and salinity variabilities is unsurprising since together they specify the density of water mass and hence affect buoyancy. The variability observed is apparently thus compatible with a pure effect of turbulence.

It is not new to state that turbulence is the underlying dominant influence on oceanic distributions. Variables of primarily physical origin, such as temperature, have spectra expected of a passive tracer in a turbulent system. However, we show quite clearly that phytoplankton must be considered as an active rather than passive scalar. First, the large-scale regime is neither pure passive nor growth dominated, but can be modelled as a complex non-linear interaction of the two, leading to a distinct scaling regime implying that patchiness is determined by both factors. In addition, there is a new high-frequency regime (corresponding to scales <100 m but quite variable) where the spectrum is significantly rougher (whiter). Since the spatial scale at which the deviations take place is quite large (~100 m) compared to the size of the organisms at hand (~100 μm) and it is known that zooplankton can have a much whiter spectrum than turbulence (Mackas *et al.*, 1985; Tsuda *et al.*, 1993), it seems possible that a non-linear coupling of a trophodynamic relationship via the functional response could explain much of this variation. Research on this topic is in progress, though scale-dependent correlations certainly complicate such analyses. Certainly, we have not seen an effect of coastal heterogeneity on the scaling behaviour of the planktonic distributions, and physical fields only seem to influence the distributions at fairly large spatial scales. To understand effectively the interactions of plankton with their environment, focus must be placed on the consequences of not only the better known physical forcers, but also the lesser understood biological influences.

ACKNOWLEDGEMENTS

We thank P. Garrido, A. Bambridge and R. Nowak for helpful discussion and some data analysis.

REFERENCES

Abraham, E. R. (1998) The generation of plankton patchiness by turbulent stirring. *Nature*, **391**, 577–580.

Austin, L. B., Austin, G. L., Schuepp, P. and Saucier, A. (1991) Atmospheric boundary layer variability and its implication for CO_2 flux measurements. In Schertzer ,S. L. D. (ed.), *Nonlinear Varaibility in Geophysics: Scaling and Fractals.* Kluwer, Boston, pp. 269–278.

Baars, M. A. and Fransz, H. G. (1984) Grazing pressure of copepods on the phytoplankton stock of the central north sea. *Neth. J. Sea Res.*, **18**, 120–142.

Brylinski, J. M., Bentley, D. and Quisthoudt, C. (1988) Discontinuité écologique et zooplankton (copépodes) en Manche Orientale. *J. Plankton Res.*, **10**, 503–513.

Capriulo, G. M. and Carpenter, E. J. (1980) Grazing by 35 to 202 mm micro-zooplankton in Long Island Sound. *Mar. Biol.*, **56**, 319–326.

Chigirinskaya, Y., Schertzer, D., Lovejoy, S., Lazarev, A. and Ordanovich, A. (1994) Unified multifractal atmospheric dynamics tested in the tropics. Part 1: horizontal scaling and self organized criticality. *Nonlin. Processes Geophys.*, **1**, 105–114.

Claereboudt, M., Lovejoy, S., Tessier, Y., Currie, J., Roff, J., Bourget, E. and Schertzer, D. (2000) Universal multifractals and ocean patchiness: a new framework. *J. Mar. Biol.*, submitted.

Currie, W. J. S., Claereboudt, M. R. and Roff, J. C. (1998) Gaps and patches in the ocean: a one-dimensional analysis of planktonic distributions. *Mar. Ecol. Prog. Ser.*, **171**, 15–21.

Daro, M. H. (1980) Field study of the diel feeding of a population of *Calanus finmarchicus* at the end of a phytoplankton bloom. *Forsch. Ergebn.*, **22**, 123–132.

Denman, K. L. and Platt, T. (1976) The variance spectrum of phytoplankton in a turbulent ocean. *J. Mar. Res.*, **34**, 593–601.

Denman, K. L., Okubo, A. and Platt, T. (1977) The chlorophyll fluctuation spectrum in the sea. *Limnol. Oceanogr.*, **22**, 1033–1038.

Finn, D., Lamb, B., Leclerc, M. Y., Lovejoy, S., Pecknold, S. and Schertzer, D. (2000) Multifractal analysis of plume concentration fluctuations in surface layer flows. *J. Appl. Meteorol.*, in press.

Folt, C. L. and Burns, C. W. (1999) Biological drivers of zooplankton patchiness. *Trends Ecol. Evol.*, **14**, 300–305.

Fransz, H. G., Miguel, J. C. and Gonzales, S. R. (1984) Mesozooplankton composition, biomass and vertical distribution and copepod production in the stratified central North Sea. *Neth. J. Sea Res.*, **18**, 82–96.

Hoch, T. and Ménesguen, A. (1997) Modelling the biogeochemical cycles of elements limiting primary production in the English Channel. II. Sensitivity analyses. *Mar. Ecol. Prog. Ser.*, **146**, 189–205.

Holligan, P. M. and Harbour, D. S. (1977) The vertical distribution and succession of phytoplankton in the western English Channel in 1975 and 1976. *J. Mar. Biol. Assoc. UK*, **57**, 1075–1093.

Kolmogorov, A. N. (1941) Local structure of turbulence in an incompressible liquid for very large Reynolds numbers. *Proc. Acad. Sci. USSR Geochem. Sect.*, **30**, 299–303.

Lazarev, A., Schertzer, D., Lovejoy, S. and Chigirinskaya, Y. (1994) Unified multifractal atmospheric dynamics tested in the tropics. Part II: vertical scaling and generalized scale invariance. *Nonlin. Processes Geophys.*, **1**, 115–123.

Lovejoy, S., Schertzer, D., Stanway, J. D., Watson, B. and Sachs, D. (1997) Multifractal modelling and analysis of radiation in clouds: 5000 km to 50 cm In *7th Atmospheric Radiation Measurements (ARM) Meeting.* US Department of Energy (DOE), San Antonio, TX, 3/97.

Lovejoy, S., Schertzer, D. and Silas, P. (1998) Diffusion on one dimensional multifractals. *Water Resour. Res.*, **34**, 3283–3291.

Lovejoy, S., Schertzer, D., Tessier, Y. and Gdonac'h, H. (2000) Multifractals and resolution independent remote sensing algorithms: the example of ocean colour. *Int. J. Remote Sensing*, in press.

Lovejoy, S., Schertzer, D. and Stanway, J. D. Direct evidence of atmospheric cascade dynamics from 1 to 20,000km. *Phys. Rev. Lett.* submitted.

Mackas, D. L., Denman, K. L. and Abbott, M. (1985) Plankton patchiness: biology in the physical vernacular. *Bull. Mar. Sci.*, **37**, 652–674.

Marguerite, C., Schertzer, D., Schmitt, F. and Lovejoy, S. (1998) Copepod diffusion within multifractal phytoplankton fields. *J. Mar. Biol.* Sys., **16**, 69–83.

Monin, A. S. and Yaglom, A. M. (1975) *Statistical Fluid Mechanics.* MIT Press, Boston, MA.

O'Neil, R. V. and King, A. W. (1998) Homage to St. Michael: or, why are there so many books on scale? In Peterson, D. L. and Parker, V. T. (eds), *Ecological Scale: Theory and Applications.* Columbia University Press, New York.

Pascual, M., Ascioti, A. and Caswell, H. (1995) Intermittency in the plankton: a multifractal analysis of zooplankton biomass variability. *J. Plankton Res.*, **17**, 1209–1232.

Pelletier, J. (1995) *Multifractal Characterization of Aircraft-Based Measurements*

of Turbulence and Passive Scalar Fields within the Surface Boundary Layer. McGill, Montreal.

Peterson, D. L. and Parker, V. T. (1998) Ecological scale: theory and applications. In O'Neil, R. V. (ed.), *Complexity in Ecological Systems*. Columbia University Press, New York.

Pinel-Alloul, B. (1995) Spatial heterogeneity as a multiscale characteristic of zooplankton communities. *Hydrobiologia*, **300/301**, 17–42.

Powell, M. T. (1995) Physical and biological scales in variability in lakes, estuaries and the coastal ocean. In Powell, T. M. and Steele, J. H. (eds), *Ecological Time Series*. Chapman and Hall, New York, pp. 119–138.

Powell, T. M. and Steele, J. H. (1995) *Ecological Time Series*. Chapman and Hall, New York.

Salvadori, G., Ratti, S. P., Belli, G., Lovejoy, S. and Schertzer, D. (1992) Multifractal objective analysis of seveso ground pollution. *Ann. Geophys.*, in press.

Schertzer, D. and Lovejoy, S. (1985a) The dimension and intermittency of atmospheric dynamics. In Launder, B. (ed.), *Turbulent Shear Flow*. Springer-Verlag, Berlin, Vol. 4, pp. 7–33.

Schertzer, D. and Lovejoy, S. (1985b) Generalised scale invariance in turbulent phenomena. *Physico-Chem. Hydrodyn. J.*, **6**, 623–635.

Schertzer, D. and Lovejoy, S. (1987) Physical modeling and analysis of rain and clouds by anisotropic scaling of multiplicative processes. *J. Geophys. Res.*, **92**, 9693–9714.

Schertzer, D. and Lovejoy, S. (1994) Multifractal generation of self-organized criticality. In Novak, M. M. (ed.), *Fractals in the Natural and Applied Sciences*. Elsevier, North-Holland, pp. 325–339.

Schertzer, D. and Lovejoy, S. (1995) From scalar cascades to Lie cascades: joint multifractal analysis of rain and cloud processes. In Feddes, R. A. (ed.), *Space/time Variability and Interdependance for Various Hydrological Processes*. Cambridge University Press, New York, pp. 153–173.

Schertzer, D. and Lovejoy, S. (1997) Universal multifractals do exist! *J. Appl. Meteorol.*, **36**, 1296–1303.

Schertzer, D., Lovejoy, S. and Lavallée, D. (1993) Generic multifractal phase transitions and self-organized criticality. In Perdang, J. M. and Lejeune, A. (eds), *Cellular Automata: Prospects in Astronomy and Astrophysics*. World Scientific, Hong Kong, pp. 216–227.

Schertzer, D., Lovejoy, S., Schmitt, F., Chigirinskaya, Y. and Marsan, D. (1997) Multifractal cascade dynamics and turbulent intermittency. *Fractals*, **5**, 427–471.

Schertzer, D., Larchvêque, M., Duan, J., Yanovsky, V. V. and Lovejoy, S. (2000) Fractional Fokker-Planck equation for non-linear stochastic differential equations divern by non-Gaussian Levy stable noises. *J. Math. Phys.*, **41**, 1–13

Schmitt, F., Lavallée, D., Schertzer, D. and Lovejoy, S. (1992a) Empirical determination of universal multifractal exponents in turbulent velocity fields. *Phys. Rev. Lett.*, **68**, 305–308.

Schmitt, F., Lovejoy, S., Schertzer, D., Lavallée, D. and Hooge, C. (1992b) First estimates of multifractal indices for velocity and temperature fields. *C.R. Acad. Sci. Paris Ser. II*, **314**, 749–754.

Schmitt, F., Schertzer, D., Lovejoy, S. and Brunet, G. (1996) Universal multifractal structure of atmospheric temperature and velocity fields. *Europhys. Lett.*, **34**, 195–200.

Seuront, L., Schmitt, F., Schertzer, D., Lagadeuc, Y. and Lovejoy, S. (1996a) Multifractal analysis of Eulerian and Lagrangian variability of physical and biological fields in the ocean. *J. Nonlin. Processes Geophys.*, **3**, 236–246.

Seuront, L., Schmitt, F., Lagadeuc, Y., Schertzer, D., Lovejoy, S. and Frontier, S. (1996b) Universal multifractal structure of phytoplankton biomass and temperature in the ocean. *Geophys. Res. Lett.*, **23**, 3591–3594.

Seuront, L., Schmitt, F., Lagadeuc, Y., Schertzer, D. and Lovejoy, S. (1999) Universal multifractal analysis as a tool to characterize multiscale intermittent patterns: example of phytoplankton distribution in turbulent coastal waters. *J. Plankton Res.*, **21**, 877–922.

Shuleykin, V. V. (1956) The theory of ocean waves. *Tr. Morskogo Gidrofiz. Inst. Akad. Nauk SSSR*, **9**, 131–149.

Stanway, J. D. (2000) Multifractal analysis of cloud radiances from 5000 to 1km. MSc Thesis, McGill University, Montreal.

Steele, J. H. (1995) Can ecological concepts span the land and ocean domains? In Powell, T. M. and Steele, J. H. (eds), *Ecological Time Series*. Chapman and Hall, New York.

Strickland, J. D. H. and Parsons, T. R. (1972) *A Practical Handbook of Seawater Analysis*, **167**. *Bull. Res. Board Can.*

Tessier, Y., Lovejoy, S., Schertzer, D., Lavallée, D. and Kerman, B. (1993) Universal multifractal indices for the ocean surface at far red wavelengths. *Geophys. Res. Lett.*, **20**, 1167–1170.

Tsuda, A., Sigisaki, H., Ishimaru, T., Saino, T. and Sato, T. (1993) White-noise-like distributions of the oceanic copepod *Neocalanus cristatus* in the subarctic North Pacific. *Mar. Ecol. Prog. Ser.*, **97**, 39–46.

Visvanathan, R., Weber, C. and Gibart, P. (1991) The stochastic coherence and the dynamics of global climate models and data. In Schertzer, D. and Lovejoy, S. (eds), *Non-linear Variability in Geophysics: Scaling and Fractals*. Kluwer, Dordrectht, pp. 269–278.

Wang, Y. (1995) Measurements and multifractal analysis of turbulent temperature and velocity near the ground. MSc Thesis, McGill University, Montreal.

Received on July 21, 1999; accepted on May 31, 2000